bioRxiv preprint doi: https://doi.org/10.1101/2024.02.01.578300; this version posted February 6, 2024. The copyright holder for this preprint (which was not certified by peer review) is the author/funder, who has granted bioRxiv a license to display the preprint in perpetuity. It is made available under aCC-BY-NC 4.0 International license.

Quantifying the fitness effects of resistance alleles with and without anthelmintic selection pressure using *Caenorhabditis elegans*

Authors: Amanda O. Shaver[1], Isabella R. Miller[1], Etta S. Schaye[1], Nicolas D. Moya[2], J.B. Collins[1], Janneke Wit[1], Alyssa H. Blanco[1], Fiona M. Shao[1], Elliot J. Andersen[1], Sharik A. Khan[1], Gracie Paredes[1], Erik C. Andersen[2]

Affiliations:

[1] Molecular Biosciences, Northwestern University, Evanston, Illinois, United States of America
[2] Dept. of Biology, Johns Hopkins University, Baltimore, Maryland, United States of America

Corresponding author:
Erik C. Andersen
Johns Hopkins University
Department of Biology
3400 N. Charles St.
Bascom UTL 383
Baltimore, MD 21218
410-516-1282
erik.andersen@gmail.com

Short Title: Fitness effects of resistance alleles in *Caenorhabditis elegans*

Keywords: Albendazole, Ivermectin, Glutamate-gated chloride channels (GluCls), *C. elegans*, Anthelmintic resistance, Competitive fitness, Fecundity, Development

ORCIDs and emails:
Amanda O. Shaver: 0000-0002-2910-1505, amandaoshaver@gmail.com
Isabella R. Miller: 0000-0002-3495-5644, miller.ir18@gmail.com
Etta S. Schaye: 0000-0003-1482-3916, etta.schaye@northwestern.edu, ettaschaye@gmail.com
Nicolas D. Moya: 0000-0002-6817-1784, nmoya1@jh.edu
J. B. Collins: 0000-0003-0808-5216, james.collins@northwestern.edu
Janneke Wit: 0000-0002-3116-744X, jannekewit@gmail.com
Alyssa H. Blanco: 0009-0001-5506-2060, alyssablanco2025@u.northwestern.edu
Fiona M. Shao: fionashao2024@u.northwestern.edu
Elliot J. Andersen: elliotjandersen@gmail.com
Sharik A. Khan: 0009-0005-3589-8134, sharikkhan2024@u.northwestern.edu, sharikakhan544@gmail.com
Gracie Paredes: gracieparedes2024@u.northwestern.edu
Erik C. Andersen: 0000-0003-0229-9651, erik.andersen@gmail.com

Journal: *PLoS Pathogens*

bioRxiv preprint doi: https://doi.org/10.1101/2024.02.01.578300; this version posted February 6, 2024. The copyright holder for this preprint (which was not certified by peer review) is the author/funder, who has granted bioRxiv a license to display the preprint in perpetuity. It is made available under aCC-BY-NC 4.0 International license.

ABSTRACT

Albendazole and ivermectin are the two most commonly co-administered anthelmintic drugs in mass-drug administration programs worldwide. Despite emerging resistance, we do not fully understand the mechanisms of resistance to these drugs nor the consequences of delivering them in combination. Albendazole resistance has primarily been attributed to variation in the drug target, a beta-tubulin gene. Ivermectin targets glutamate-gated chloride channel (GluCl) genes, but it is unknown whether these genes are involved in ivermectin resistance in nature. Using *Caenorhabditis elegans*, we defined the fitness costs associated with loss of the drug target genes singly or in combinations of the genes that encode GluCl subunits. We quantified the loss-of-function effects on three traits: (i) multi-generational competitive fitness, (ii) fecundity, and (iii) development. In competitive fitness and development assays, we found that a deletion of the beta-tubulin gene *ben-1* conferred albendazole resistance, but ivermectin resistance required loss of two GluCl genes (*avr-14* and *avr-15*) or loss of three GluCl genes (*avr-14*, *avr-15*, and *glc-1*). The fecundity assays revealed that loss of *ben-1* did not provide any fitness benefit in albendazole and that no GluCl deletion mutants were resistant to ivermectin. Next, we searched for evidence of multi-drug resistance across the three traits. Loss of *ben-1* did not confer resistance to ivermectin, nor did loss of any single GluCl subunit or combination confer resistance to albendazole. Finally, we assessed the development of 124 *C. elegans* wild strains across six benzimidazoles and seven macrocyclic lactones to identify evidence of multi-drug resistance between the two drug classes and found a strong phenotypic correlation within a drug class but not across drug classes. Because each gene affects various aspects of nematode physiology, these results suggest that it is necessary to assess multiple fitness traits to evaluate how each gene contributes to anthelmintic resistance.

bioRxiv preprint doi: https://doi.org/10.1101/2024.02.01.578300; this version posted February 6, 2024. The copyright holder for this preprint (which was not certified by peer review) is the author/funder, who has granted bioRxiv a license to display the preprint in perpetuity. It is made available under aCC-BY-NC 4.0 International license.

AUTHOR SUMMARY

Control of parasitic nematodes often depends on mass-drug administration (MDA) programs, where combinations of anthelmintics are distributed to at-risk populations. Two commonly co-administered anthelmintic drugs in MDA programs are albendazole and ivermectin, and resistance to both drugs has emerged. Although the mechanism of resistance (MoR) to albendazole has been primarily attributed to variation in a beta-tubulin gene, the MoR to ivermectin remains unknown. Ivermectin acts through pentameric glutamate-gated chloride channels (GluCls). However, it is unclear whether genes that encode GluCls are involved in ivermectin resistance in parasitic nematodes. Using *Caenorhabditis elegans*, we quantified the fitness costs associated with deletions of the beta-tubulin gene *ben-1* and three genes encoding GluCl subunits *avr-14*, *avr-15*, and *glc-1* on three traits: (i) multi-generational competitive fitness, (ii) fecundity, and (iii) development. We found different anthelmintic responses across strains and traits but no evidence of multi-drug resistance. Our results suggest that multiple traits should be considered to understand resistance comprehensively and that the determination of whether a gene plays a role in anthelmintic resistance depends on the trait measured. Understanding the quantitative effects and fitness-associated costs of each GluCl subunit in *C. elegans* can help explain the costs of mutations in these subunits in parasites.

bioRxiv preprint doi: https://doi.org/10.1101/2024.02.01.578300; this version posted February 6, 2024. The copyright holder for this preprint (which was not certified by peer review) is the author/funder, who has granted bioRxiv a license to display the preprint in perpetuity. It is made available under aCC-BY-NC 4.0 International license.

INTRODUCTION

Parasitic nematodes are some of the most abundant, diverse, and destructive parasites of humans that cause significant socio-economic and health impacts, including the collective loss of over eight million disability-adjusted life years (DALYs) [1–3]. Control of these parasites often depends on mass-drug administration (MDA) programs, where anthelmintics are distributed in combinations to at-risk populations. However, anthelmintic resistance has emerged with reports of reduced drug efficacy against nematodes in humans, which threatens our ability to control parasitic nematode infections [4–8]. In veterinary medicine, overuse of anthelmintics has placed strong selective pressures on parasites, which has led to the evolution of resistance to all major drug classes [9–11] and highlights the potential for a similar pattern of anthelmintic resistance to spread throughout human parasitic nematode populations.

Simultaneous treatment with two or more drugs (*i.e.*, co-administration) from different anthelmintic classes is one method used to slow the development of resistance when a single anthelmintic has reduced efficacy [12,13]. Anthelmintic rotation, another method to slow resistance, uses the periodic switching of drug classes to alleviate selection pressures on one drug class and prolong drug lifespan and efficacy [14]. Despite the successes of both strategies, co-administration and anthelmintic rotation pose the risk of multi-drug resistance [15–17], particularly if a shared mechanism confers resistance to both drugs (*e.g.*, drug export) [18], a phenomenon known as cross-resistance [17]. Although empirical evidence for cross-resistance is lacking, its potential occurrence could increase the development of resistance to both drugs. However, neither co-administration nor anthelmintic rotation alone are enough to slow the spread of resistance. To date, various accounts of multi-drug resistance have been reported in veterinary medicine [9–11]. Therefore, it is critical to define and address the mechanisms of resistance (MoR) for each drug in a treatment plan to ensure that drug efficacy can be reached and to prevent multi-drug resistance.

bioRxiv preprint doi: https://doi.org/10.1101/2024.02.01.578300; this version posted February 6, 2024. The copyright holder for this preprint (which was not certified by peer review) is the author/funder, who has granted bioRxiv a license to display the preprint in perpetuity. It is made available under aCC-BY-NC 4.0 International license.

Two of the most commonly used anthelmintic drugs in MDA programs are albendazole, a benzimidazole (BZ), and ivermectin, a macrocyclic lactone (ML) [19–22], where these two drugs are regularly co-administered as a chemotherapeutic treatment for intestinal helminths and lymphatic filariasis [23]. Because albendazole and ivermectin are two drugs on the World Health Organization (WHO) Model Lists of Essential Medicines [23–26], it is critical to identify the MoR for both drugs to inform appropriate administration and slow the development of resistance. However, anthelmintic resistance in parasites can be difficult to disentangle because of multiple factors, including a lack of access to relevant life stages and *in vitro* culture systems, dependence on vertebrate hosts, and a limited molecular toolkit (*e.g.*, gene knockouts and induced mutations cannot be used to study genes associated with resistance in parasites) [27]. With its ease of growth, outstanding genetic tractability, and molecular toolkits, the free-living nematode *Caenorhabditis elegans* has contributed to the identification and characterization of the MoA and MoR of all major anthelmintic drug classes [27–34]. Additionally, wild *C. elegans* strains from the *Caenorhabditis* Natural Diversity Resource (CaeNDR) [35] have been used to explore anthelmintic resistance in natural populations and to uncover novel MoR [30,35–42].

Both the laboratory-adapted strain, N2, and *C. elegans* wild strains have facilitated the identification and characterization of the beta-tubulin gene *ben-1* as the primary target of albendazole and other BZs [28,29,39,42,43]. Loss-of-function mutations in *ben-1* have been identified in *C. elegans* strains resistant to BZs [44]. Furthermore, resistance alleles corresponding to point mutations in *ben-1* homologs in parasitic nematode populations continue to be identified [29,43,45,46]. Notably, the redundancy among the six beta-tubulin genes in *C. elegans* allows strains with a non-functional *ben-1* gene to develop normally [44]. To date, beta-tubulins have been the most well characterized anthelmintic target across nematodes [44,47–52].

Ivermectin acts as a positive allosteric modulator that selectively opens inhibitory glutamate-gated chloride channels (GluCls) in the membranes of pharyngeal muscles, motor

bioRxiv preprint doi: https://doi.org/10.1101/2024.02.01.578300; this version posted February 6, 2024. The copyright holder for this preprint (which was not certified by peer review) is the author/funder, who has granted bioRxiv a license to display the preprint in perpetuity. It is made available under aCC-BY-NC 4.0 International license.

neurons, female reproductive tracts, and the excretory/secretory pores [53–56]. However, the relationship between GluCls and the MoR of ivermectin is poorly understood. In *C. elegans*, GluCls are thought to be homopentameric or heteropentameric transmembrane complexes where six genes encode GluCl subunits: *avr-14*, *avr-15*, *glc-1*, *glc-2*, *glc-3*, and *glc-4* [57–60]. Although it is established that GluCl subunits are the main targets of ivermectin in *C. elegans*, null mutations in *avr-14*, *avr-15*, or *glc-1* individually do not cause ivermectin resistance [60]. However, mutagenesis studies of *C. elegans* showed that a triple GluCl mutant strain (*avr-14; avr-15 glc-1*) displayed greater than 4000-fold resistance and that a double GluCl mutant strain (*avr-14; avr-15*) had intermediate levels of resistance as compared to the wild-type strain [60]. This study demonstrated that mutations in multiple GluCl subunit genes can cause high-level ivermectin resistance. Nevertheless, it is essential to note that the mutagenesis studies in *C. elegans* were not performed in a controlled background and assessed only one trait, survival, as measured by placing embryos on agar plates with ivermectin and observing the number of embryos that grew to adulthood [58,60]. It is important to assess multiple traits to evaluate ivermectin resistance because GluCls are widely expressed across several tissue types in the *C. elegans* nervous system and pharynx [61,62]. To adequately evaluate the MoR to ivermectin, fitness, development, and fecundity can be used to understand how GluCl subunit genes interact and play a role in resistance and, ultimately, assess how they could affect the spread of resistance alleles in parasite populations.

Using *C. elegans*, we defined the fitness costs associated with the loss of *ben-1*, *avr-14*, *avr-15*, and *glc-1* and the loss of combinations of GluCl subunits all in a controlled genetic background on nematode resistance to albendazole and ivermectin. We measured three fitness components: (i) multi-generational competitive fitness, (ii) fecundity, and (iii) development. First, in the competitive fitness assay, we found that loss of *ben-1* conferred albendazole resistance, and loss of GluCl subunits did not confer albendazole resistance. We found that loss of *avr-15* carried significant fitness consequences when not under drug selection pressure. Under constant

bioRxiv preprint doi: https://doi.org/10.1101/2024.02.01.578300; this version posted February 6, 2024. The copyright holder for this preprint (which was not certified by peer review) is the author/funder, who has granted bioRxiv a license to display the preprint in perpetuity. It is made available under aCC-BY-NC 4.0 International license.

ivermectin exposure, loss of both *avr-14* and *avr-15* and all three GluCl subunits (*avr-14*, *avr-15*, and *glc-1*) caused strong selective advantages compared to the wild-type strain. Second, in the fecundity assays, we found that loss of *ben-1* did not confer any advantage in the presence of albendazole and that all strains with an *avr-15* deletion had reduced fecundity in all conditions compared to the wild-type strain. Third, in our assessment of development, we found that loss of *ben-1* conferred resistance to albendazole, and loss of both *avr-14* and *avr-15* or all three GluCl subunits conferred ivermectin resistance. Fourth, we sought to identify any evidence of cross-resistance between albendazole and ivermectin by comparing the fitness costs of each deletion mutant strain in both drugs. Across the three fitness traits we assessed, we found that the *ben-1* deletion mutant strain did not confer resistance in the presence of ivermectin, nor did the GluCl deletion mutant strains display resistance in the presence of albendazole. Fifth, we assessed the development of 124 *C. elegans* wild strains across six BZs and seven MLs to identify evidence of cross-resistance between the two drug classes in natural populations. We found a strong correlation with phenotype within a drug class but not across drug classes, which indicates that phenotypic responses to the two drug classes are distinct, likely because they target different aspects of nematode development. Here, we present a comprehensive study that assessed the quantitative effects that *ben-1* and GluCl mutations have on various aspects of nematode fitness in the presence of albendazole or ivermectin. These results suggest that conclusions about a gene's involvement in anthelmintic resistance depend on the trait assessed and that multiple fitness traits must be considered to understand resistance comprehensively.

RESULTS

Multi-generational competitive fitness assays show how loss of beta-tubulin and GluCl subunits are selected in control or anthelmintic conditions

CRISPR-Cas9 genome editing was performed to generate four deletion strains that each cause loss of function. Each strain contains a single deletion in either the beta-tubulin gene, *ben-*

bioRxiv preprint doi: https://doi.org/10.1101/2024.02.01.578300; this version posted February 6, 2024. The copyright holder for this preprint (which was not certified by peer review) is the author/funder, who has granted bioRxiv a license to display the preprint in perpetuity. It is made available under aCC-BY-NC 4.0 International license.

187 *1*, or the GluCl subunit genes *avr-14*, *avr-15*, or *glc-1* (**Fig 1**, **Table S1**). Next, to comprehensively
188 assess the role that *avr-14*, *avr-15*, and *glc-1* play in ivermectin resistance, we created double
189 mutants of each combination of GluCl deletion alleles and a triple mutant (*avr-14; avr-15 glc-1*)
190 by crossing the single deletion strains (see *Methods*). We performed competitive fitness assays
191 to determine the selective advantages or disadvantages of alleles in control or drug treatment
192 conditions. Fitness involves the ability of an organism, or population, to survive and reproduce in
193 its environment [63,64]. In these assays, a query strain was competed against the barcoded wild-
194 type strain PTM229 (**Table S1**), which contains a synonymous change in the *dpy-10* locus in the
195 N2 background and does not cause any fitness effects compared to the normal laboratory N2
196 strain [65] in the presence of dimethyl sulfoxide (DMSO), albendazole, or ivermectin (**Fig S1)**.
197 Because all query strains contain the wild-type *dpy-10* locus, allele frequencies of *dpy-10* between
198 PTM229 and each query strain were measured for each generation to quantify relative fitness.

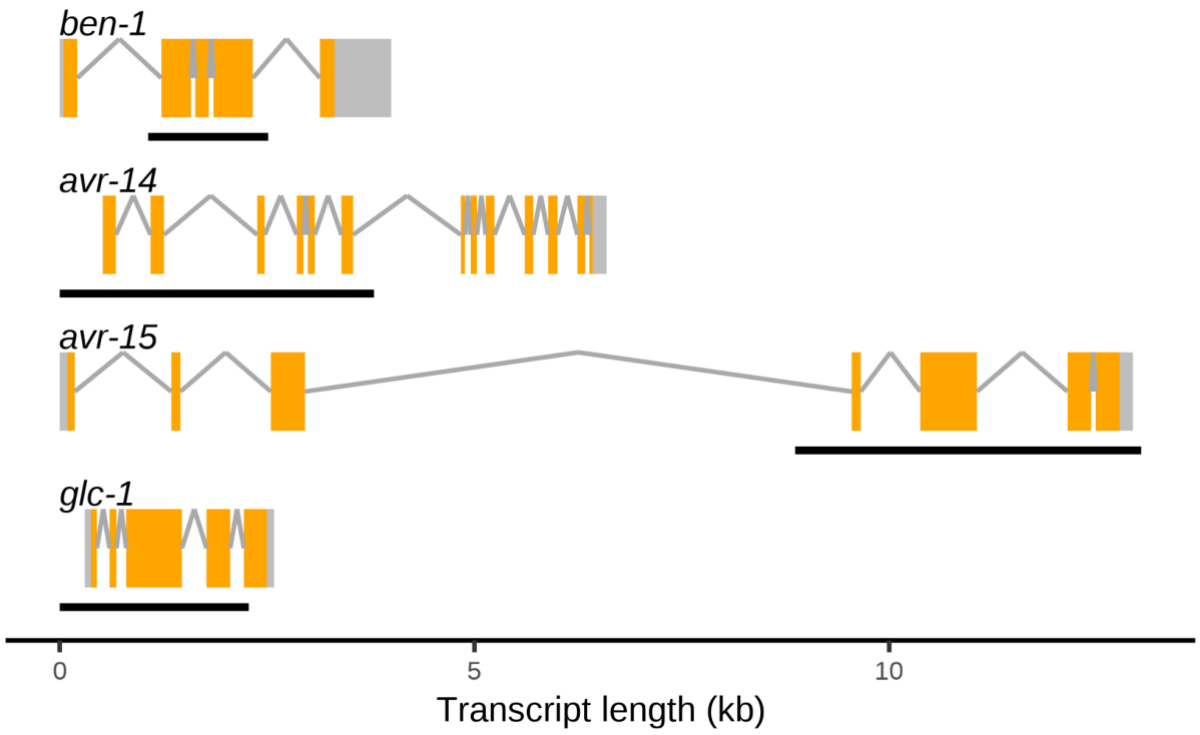

bioRxiv preprint doi: https://doi.org/10.1101/2024.02.01.578300; this version posted February 6, 2024. The copyright holder for this preprint (which was not certified by peer review) is the author/funder, who has granted bioRxiv a license to display the preprint in perpetuity. It is made available under aCC-BY-NC 4.0 International license.

Fig 1. Gene models of *ben-1* and the three genes encoding for GluCl subunits in *C. elegans*
Predicted gene models presented for *ben-1*, *avr-14*, *avr-15*, and *glc-1* include exons (orange rectangles) and introns (gray lines) in the *C. elegans* laboratory-adapted strain N2 background (WS283). Black bars underneath each gene display the span of the deletion present in each gene for the strains assayed (**Table S1**).

The competitive fitness assays enabled us to focus on two key traits critical to nematode fitness: time to reproduction and reproductive rate. These assays allow us to observe small effects on nematode fitness over multiple generations. If an allele confers a deleterious fitness effect compared to the wild-type allele, then that strain will decrease in frequency over the generations. Conversely, if an allele confers a beneficial effect compared to the wild-type allele, then that strain will increase in frequency over the generations. Finally, if an allele has no difference in effect when compared to the wild-type allele, then the two strains will be found at approximately equal frequencies throughout the competitive fitness assay.

In control conditions, the wild-type strain, N2, showed no differences in competitive fitness compared to the barcoded wild-type control strain, PTM229, as expected. The loss of *ben-1*, *avr-14*, or *glc-1* in single deletion mutants, along with the loss of both *avr-14* and *glc-1* in the double mutant strain, did not have significant differences in competitive fitness as compared to the control strain, which suggests that a deletion in these genes, in control conditions, did not cause fitness consequences (**Fig 2A, Fig 2B, Fig S2**). Notably, all strains with a loss of *avr-15*, whether it be a single, double, or triple GluCl mutant, were vastly unfit and ceased to exist in the population by the third generation (**Fig 2A**). These results suggest that, when not under drug selection pressure, loss of *avr-15* is incredibly detrimental to animal fitness. Therefore, it is unlikely that individuals with *avr-15* loss-of-function alleles will be observed in natural populations.

bioRxiv preprint doi: https://doi.org/10.1101/2024.02.01.578300; this version posted February 6, 2024. The copyright holder for this preprint (which was not certified by peer review) is the author/funder, who has granted bioRxiv a license to display the preprint in perpetuity. It is made available under aCC-BY-NC 4.0 International license.

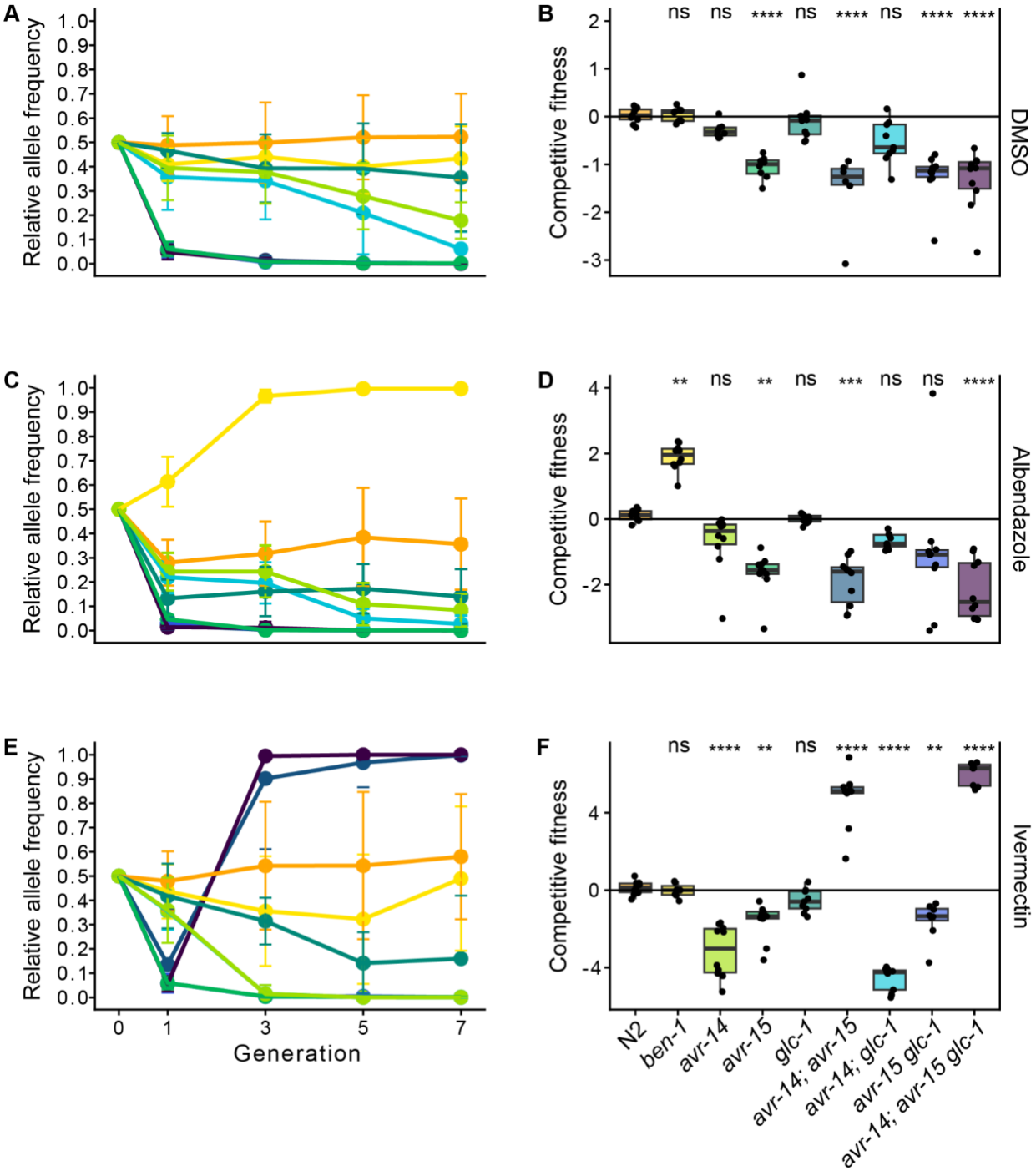

Fig 2. Competitive fitness assays across seven generations in DMSO, albendazole, and ivermectin.
A barcoded N2 wild-type strain, PTM229, was competed with strains that have deletions in either one, two, or three genes that encode GluCl channels or the beta-tubulin gene *ben-1* in **(A)** DMSO, **(C)** albendazole, and **(E)** ivermectin. Generation is shown on the x-axis, and the relative allele frequencies of the nine strains with genome-edited alleles and N2 are shown on the y-axis. The log_2-transformed competitive fitness of each allele is plotted in **(B)** DMSO, **(D)** albendazole, and **(F)** ivermectin. The gene tested is shown on the x-axis, and the competitive fitness is shown on

bioRxiv preprint doi: https://doi.org/10.1101/2024.02.01.578300; this version posted February 6, 2024. The copyright holder for this preprint (which was not certified by peer review) is the author/funder, who has granted bioRxiv a license to display the preprint in perpetuity. It is made available under aCC-BY-NC 4.0 International license.

the y-axis. Each point represents a biological replicate of that competition experiment. Data are shown as Tukey box plots with the median as a solid horizontal line, and the top and bottom of the box representing the 75th and 25th quartiles, respectively. The top whisker is extended to the maximum point that is within the 1.5 interquartile range from the 75th quartile. The bottom whisker is extended to the minimum point that is within the 1.5 interquartile range from the 25th quartile. Significant differences between the wild-type N2 strain and all the other alleles are shown as asterisks above the data from each strain ($p > 0.05$ = ns, $p < 0.001$ = ***, $p < 0.0001$ = ****, Tukey HSD). Because two DMSO competitive fitness assays were performed, results from both DMSO assays are reported (**S2 Fig**).

In drug conditions, we can assess whether loss of any of these genes causes resistance. In albendazole conditions, the loss of *ben-1* caused a strong fitness advantage over the control strain and swept to fixation in the population by the third generation (**Fig 2C, Fig 2D**). Notably, the loss of one, two, or all three GluCl genes caused a reduction of fitness in albendazole conditions, and each strain displayed a similar competitive fitness response in albendazole as observed in control conditions (**Fig 2C, Fig 2D**). In ivermectin conditions, the loss of *ben-1* or *glc-1* caused no significant differences in competitive fitness as compared to the control strain. The loss of *avr-14* or *avr-15*, the loss of both *avr-14* and *glc-1*, or the loss of both *avr-15* and *glc-1* caused significantly reduced competitive fitness in ivermectin compared to the control strain (**Fig 2E, Fig 2F**). By contrast, the loss of both *avr-14* and *avr-15* and the loss of all three GluCl genes (*avr-14*, *avr-15*, and *glc-1*) caused strains to sweep to fixation in the presence of ivermectin by the third generation, indicating that they had significantly improved fitness as compared to the control strain (**Fig 2E**). Results from these competitive fitness assays suggest that ivermectin resistance is only observed when both *avr-14* and *avr-15* functions are lost. The fitness disadvantages of losing *avr-14* or *avr-15* alone outweigh any ivermectin resistance that could be present. The loss of *glc-1* in addition to loss of both *avr-14* and *avr-15* caused the triple mutant strain to sweep to fixation faster than the *avr-14; avr-15* double mutant strain. However, these two strains did not significantly differ in competitive fitness.

Fecundity effects caused by loss of beta-tubulin or GluCl subunits in control or anthelmintic conditions

bioRxiv preprint doi: https://doi.org/10.1101/2024.02.01.578300; this version posted February 6, 2024. The copyright holder for this preprint (which was not certified by peer review) is the author/funder, who has granted bioRxiv a license to display the preprint in perpetuity. It is made available under aCC-BY-NC 4.0 International license.

To dissect the genetic basis of anthelmintic resistance, we must identify the roles of *ben-1* and the GluCl subunit genes in nematode fecundity and their potential influence on the spread and persistence of resistance alleles in a population. As a measure of relative fitness, fecundity refers to the number of offspring produced by an organism [63,64]. To compare the effects on fecundity caused by the loss of *ben-1* and the GluCl subunit genes, we measured lifetime fecundity, daily fecundity, and intrinsic growth rate of the nine *C. elegans* strains (see *Methods*). Single L4 larval stage hermaphrodites were placed on NGMA plates under control (DMSO), albendazole, or ivermectin conditions [66]. Hermaphrodites were transferred every 24 hours for five days and maintained under standard laboratory conditions. After five days, hermaphrodites were transferred for the final time to a new NGMA plate for 48 hours. We manually counted the offspring from images of assay plates from single hermaphrodites. The results showed considerable differences in lifetime fecundity among the nine strains across the three conditions (**Fig 3**).

bioRxiv preprint doi: https://doi.org/10.1101/2024.02.01.578300; this version posted February 6, 2024. The copyright holder for this preprint (which was not certified by peer review) is the author/funder, who has granted bioRxiv a license to display the preprint in perpetuity. It is made available under aCC-BY-NC 4.0 International license.

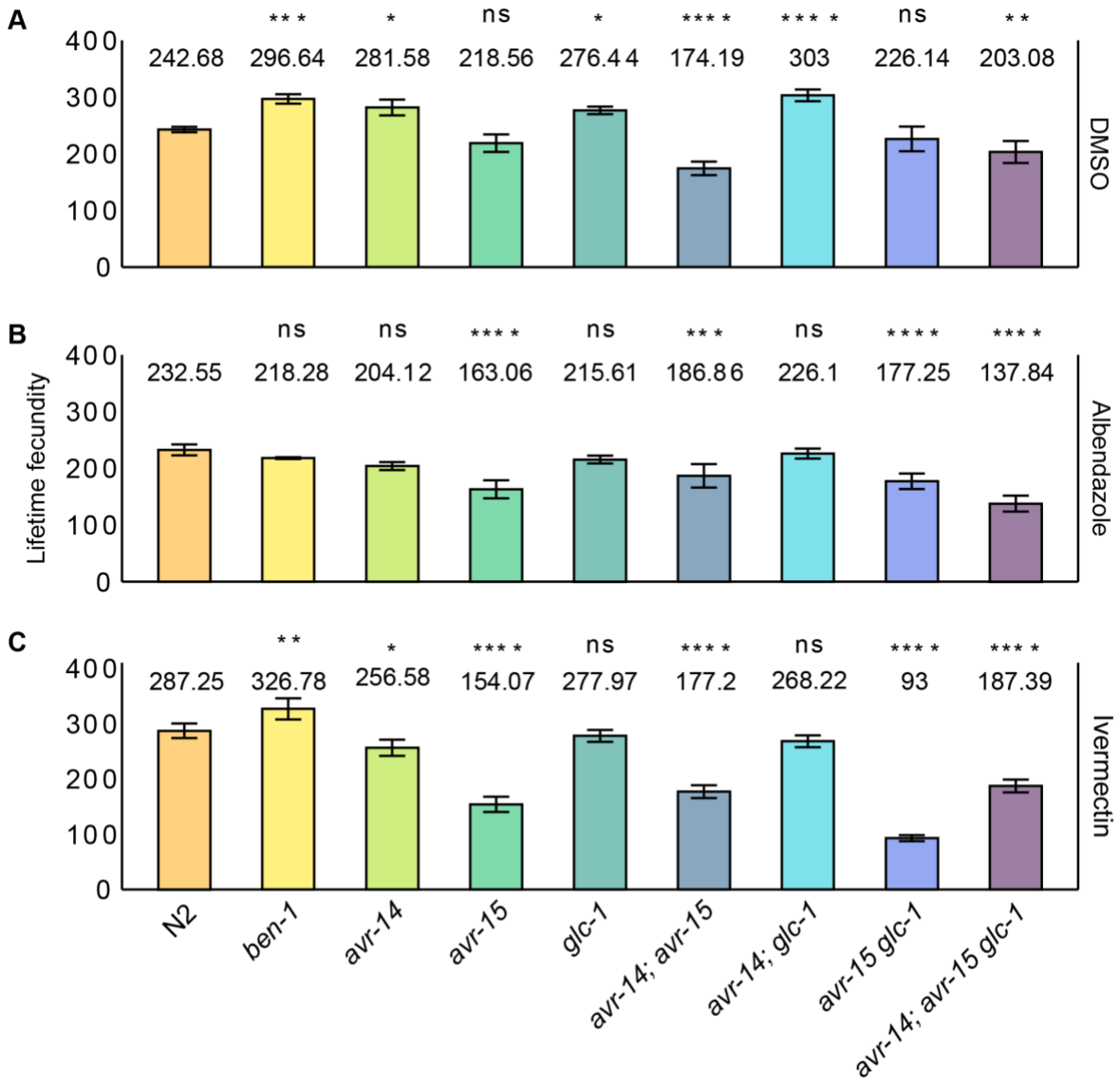

Fig 3. Variation in lifetime fecundity of beta-tubulin and GluCl mutants in the presence of DMSO, albendazole, or ivermectin.
Bar plots for lifetime fecundity, y-axis, for each deletion strain on the x-axis in **(A)** DMSO, **(B)** albendazole, and **(C)** ivermectin are shown. Error bars show the standard deviation of lifetime fecundity among 7 - 10 replicates. The laboratory reference strain, N2, is colored orange. Other strains are colored by genotype. Comparisons of lifetime fecundity between the laboratory reference strain, N2, and all deletion strains are shown. Statistical significance was calculated using Tukey HSD. Significance of each comparison is shown above each comparison pair ($p > 0.05$ = ns, $p < 0.05$ = *, $p < 0.01$ = **, $p < 0.001$ = ***, $p < 0.0001$ = ****, Tukey HSD).

Fecundity directly impacts population growth rate and survival. Measuring fecundity provides insights into reproductive success, which is fundamental to the assessment of animal fitness and resilience when exposed to environmental changes. Here, the fecundity assays

bioRxiv preprint doi: https://doi.org/10.1101/2024.02.01.578300; this version posted February 6, 2024. The copyright holder for this preprint (which was not certified by peer review) is the author/funder, who has granted bioRxiv a license to display the preprint in perpetuity. It is made available under aCC-BY-NC 4.0 International license.

enabled us to focus on offspring production both in control conditions and under constant drug selection pressure. By assessing fecundity in control (DMSO) conditions, we can discern the fitness effects caused by loss of *ben-1* or by the loss of GluCl subunit genes when not under drug selection pressure. The loss of *ben-1* caused increased fecundity (**Fig 3A**), which suggests that *ben-1* limits fecundity in control conditions. The loss of *avr-15* alone and loss of both *avr-15* and *glc-1* did not affect lifetime fecundity as compared to the N2 strain. However, the loss of *avr-15* in combination with *avr-14* or in combination with *avr-14* and *glc-1* caused significantly reduced lifetime fecundities as compared to the N2 strain, which suggests that in combination *avr-14* and *avr-15* or *avr-14*, *avr-15*, and *glc-1* are necessary for normal fecundity in control conditions (**Fig 3**). By contrast, the loss of *avr-14* or *glc-1* and the loss of both genes caused significantly increased lifetime fecundities as compared to the N2 strain, which suggests that *avr-14* and *glc-1* limit fecundity in control conditions.

By evaluating fecundity under drug conditions, we can uncover the fitness effects caused by mutations in *ben-1* or the GluCl subunit genes and determine how these mutations under drug pressure could affect the spread of potential resistance alleles in a population. In the presence of albendazole, the loss of *ben-1* did not cause a significant effect on lifetime or daily fecundity as compared to the N2 strain, which suggests that *ben-1* does not confer albendazole sensitivity by alteration of nematode fecundity (**Fig 3B, S4 Fig**). However, in the presence of ivermectin, the loss of *ben-1* had a significant increase in lifetime fecundity compared to the control strain, exhibiting the same pattern observed in control conditions (**Fig 3C, S5 Fig**). The loss of *glc-1* and the loss of both *avr-14* and *glc-1* did not cause significant differences in lifetime or daily fecundity compared to the N2 strain in albendazole or ivermectin, which suggests that *glc-1* alone or in combination with *avr-14* are necessary for normal fecundity production under drug pressure. By contrast, a loss of *avr-14* alone caused significantly reduced fecundity compared to the control strain in ivermectin, which indicates that *avr-14* is necessary for fecundity in ivermectin. Additionally, the loss of *avr-15* alone, the loss of both *avr-14* and *avr-15* or *avr-15* and *glc-1*, or

bioRxiv preprint doi: https://doi.org/10.1101/2024.02.01.578300; this version posted February 6, 2024. The copyright holder for this preprint (which was not certified by peer review) is the author/funder, who has granted bioRxiv a license to display the preprint in perpetuity. It is made available under aCC-BY-NC 4.0 International license.

the loss of all three GluCl subunits caused significantly reduced lifetime fecundity compared to the control strain, a trend observed across all conditions, which suggests that *avr-14* and *avr-15* alone or in combination these GluCl genes are necessary for normal fecundity. Although the loss of *avr-15* in the single, double, or triple mutant strains caused a reduction in fecundity across conditions, the daily fecundity patterns varied across the three conditions (**S3 Fig, S4 Fig, S5 Fig**). In all three conditions, strains with a loss of *avr-15* had a reduction in daily fecundity between days two and three compared to the N2 strain. In DMSO and ivermectin, strains with a loss of *avr-15* had an increase in daily fecundity between days five and seven at the end of the assay (**S4 Fig**). Because strains with a loss of both *avr-14* and *avr-15* and a loss of all three GluCl subunits have significantly reduced fecundity across all conditions, it would be unlikely for animals in nature to acquire loss-of-function mutations in these genes that cause detrimental fitness consequences.

Loss of *ben-1* conferred albendazole resistance, and loss of both *avr-14* and *avr-15* or all three GluCl subunits conferred ivermectin resistance

We then performed high-throughput assays (HTAs) to measure nematode length, a proxy for development, in strains with a loss of *ben-1* or loss of GluCl subunit genes (**Table S2**) in response to drug treatment. The assay included 72 replicates per strain with 5-30 animals per replicate in each drug or control condition. The reported nematode length of each strain is the delta between animal lengths in control and drug conditions to obtain normalized animal length and assess drug effects. Longer median animal length (*i.e.*, larger animals) than the N2 strain corresponds to increased resistance to the tested drugs, and shorter median animal length (*i.e.*, smaller animals) than the N2 strain corresponds to increased sensitivity to the tested drugs. Strains varied in length after growth for 48 hours in control conditions, but the loss of *avr-14* and *avr-15* caused the most significant delays in development (**S6 Fig**). Despite substantial variation

bioRxiv preprint doi: https://doi.org/10.1101/2024.02.01.578300; this version posted February 6, 2024. The copyright holder for this preprint (which was not certified by peer review) is the author/funder, who has granted bioRxiv a license to display the preprint in perpetuity. It is made available under aCC-BY-NC 4.0 International license.

among strains in control (DMSO) conditions, animal measurements were categorized as the L4 larval stage by our custom CellProfiler worm models.

As previously reported, the N2 strain was developmentally delayed in albendazole, where animals were shorter than in control conditions, demonstrating sensitivity to albendazole [29,39]. By contrast, the loss of *ben-1* caused albendazole resistance as demonstrated by longer animal length than observed in the N2 strain (**Fig 4A**). Although each GluCl deletion mutant strain had significantly longer animal lengths than the N2 strain, none of the seven GluCl deletion mutant strains conferred albendazole resistance as observed in the *ben-1* deletion mutant (**Fig 4A**). In ivermectin, the N2 strain had the greatest delay in development. Although, a loss of *avr-14* or *avr-15* alone or a loss of *avr-14* and *glc-1* or *avr-15* and *glc-1* in combination had significantly longer median animal lengths than the N2 strain in ivermectin (**Fig 4B**). However, the loss of a*vr-14* and *avr-15* or the loss of *avr-14*, *avr-15*, and *glc-1* caused quantitative ivermectin resistance as compared to the N2 strain. This ivermectin resistance confirms previous findings [60]. However, we did not see a significant difference in median animal length between the double GluCl mutant *avr-14* and *avr-15* or the triple GluCl mutant, as reported previously [60]. A higher concentration of ivermectin (500 nM) was also measured and confirmed the same patterns described above (**S7 Fig**).

bioRxiv preprint doi: https://doi.org/10.1101/2024.02.01.578300; this version posted February 6, 2024. The copyright holder for this preprint (which was not certified by peer review) is the author/funder, who has granted bioRxiv a license to display the preprint in perpetuity. It is made available under aCC-BY-NC 4.0 International license.

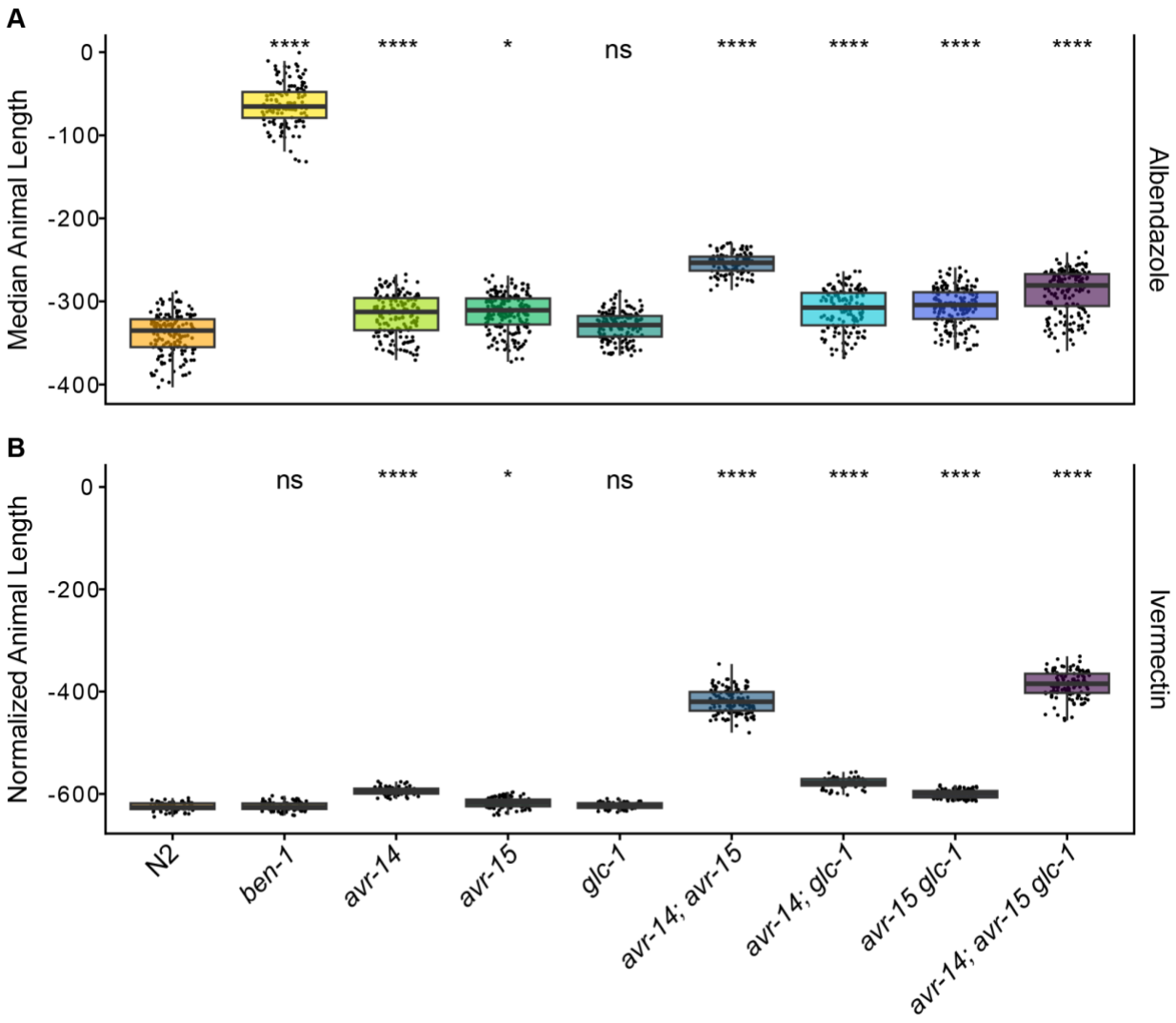

Fig 4. High-throughput assays for each mutant strain in the presence of albendazole and ivermectin.
The regressed median animal length values for populations of nematodes growth in either **(A)** 30 μM albendazole or **(B)** 250 nM ivermectin are shown on the y-axis. Each point represents the normalized median animal length value of a well containing approximately 5-30 animals. Data are shown as Tukey box plots with the median as a solid horizontal line, and the top and bottom of the box representing the 75th and 25th quartiles, respectively. The top whisker is extended to the maximum point that is within the 1.5 interquartile range from the 75th quartile. The bottom whisker is extended to the minimum point that is within the 1.5 interquartile range from the 25th quartile. Significant differences between the wild-type strain and all other deletions are shown as asterisks above the data from each strain ($p > 0.05$ = ns, $p < 0.001$ = ***, $p < 0.0001$ = ****, Tukey HSD).

No evidence of cross-resistance or multi-drug resistance between BZs and MLs

bioRxiv preprint doi: https://doi.org/10.1101/2024.02.01.578300; this version posted February 6, 2024. The copyright holder for this preprint (which was not certified by peer review) is the author/funder, who has granted bioRxiv a license to display the preprint in perpetuity. It is made available under aCC-BY-NC 4.0 International license.

Because albendazole and ivermectin are routinely distributed together to at-risk populations, it is critical to ensure that the two drugs do not have the same MoR to avoid the possibility of cross-resistance. Because we compared the response of the *ben-1* deletion mutant strain in ivermectin and all GluCl deletion mutant strains in albendazole for all fitness assays, we obtained a comprehensive picture of how these genes interact in the presence of a drug that is not designed to affect their given target. In the competitive fitness and HTAs, the loss of *ben-1* did not cause ivermectin resistance. Additionally, none of the GluCl deletion mutant strains conferred resistance to albendazole across the competitive fitness and HTAs, as compared to a loss of *ben-1*. However, it is important to note that a loss of *ben-1* did confer a slight advantage compared to the N2 strain in the ivermectin fecundity assay (**Fig 3C**). AllGluCl deletion mutant strains, except the *glc-1* deletion mutant strain, conferred a slight advantage compared to the N2 strain in the albendazole HTA (**Fig 4A**). However, it is essential to note that the competitive fitness assays did not display any evidence of cross-resistance (**Fig 2**).

Our fitness assays showed how *ben-1*, *avr-14*, *avr-15*, and *glc-1* respond under drug pressure, but we know that these genes do not account for all of the albendazole or ivermectin resistance found across the *C. elegans* species [41,43]. Therefore, we performed an HTA (see *Methods*) to assess the nematode development of 124 wild strains in the presence of six BZs and seven MLs, which included albendazole and ivermectin. We used a Spearman's Rank correlation test to test any evidence of multi-drug resistance among the BZs and MLs. We find much stronger phenotypic correlations of responses within the same drug class than we do between drug classes (**Fig 5**), and no significant correlations exist across the two drug classes (**Table S3**), which suggests that we did not detect evidence of multi-drug resistance between the two drug classes.

bioRxiv preprint doi: https://doi.org/10.1101/2024.02.01.578300; this version posted February 6, 2024. The copyright holder for this preprint (which was not certified by peer review) is the author/funder, who has granted bioRxiv a license to display the preprint in perpetuity. It is made available under aCC-BY-NC 4.0 International license.

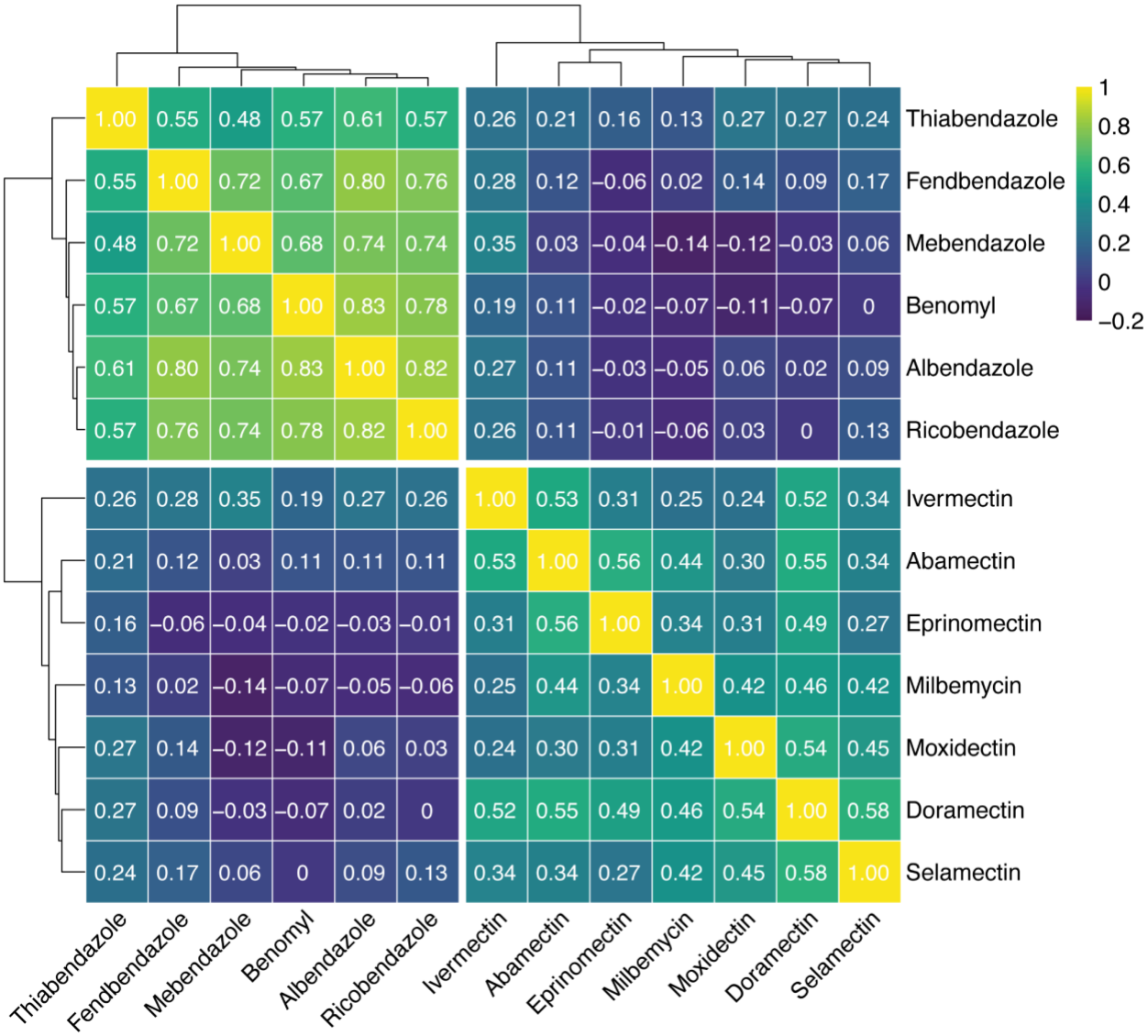

Fig 5. Spearman-rank correlations between 124 wild isolates exposed to BZs and MLs. Spearman-rank correlations and significance testing were performed between 124 wild isolates exposed to six BZs and seven MLs. The dendrograms were constructed using Euclidean distance and complete linkage metrics and then split into their two largest clusters to show the relationships of similarities between the 124 wild strains exposed to the two major anthelmintic classes. A correlation of 1 signifies the strongest phenotypic correlation (*i.e.*, identical median animal lengths) and a correlation of -0.2 signifies the weakest phenotypic correlation (*i.e.*, dissimilar median animal lengths). Significant correlations ($p < 0.05$) were recorded (**Table S3**).

bioRxiv preprint doi: https://doi.org/10.1101/2024.02.01.578300; this version posted February 6, 2024. The copyright holder for this preprint (which was not certified by peer review) is the author/funder, who has granted bioRxiv a license to display the preprint in perpetuity. It is made available under aCC-BY-NC 4.0 International license.

DISCUSSION

Here, we assessed multiple fitness traits to understand how *ben-1* and genes that encode GluCl subunits contribute to albendazole and ivermectin resistance. Additionally, the quantitative assessment of *avr-14*, *avr-15*, and *glc-1* in ivermectin response is critical to understand how GluCl subunits affect fitness in nematode populations. Because *C. elegans* shares the major characteristics of the parasitic nematode body plan, such as the cuticle and organization of the nervous system, along with a conserved neuromuscular system and neurotransmitters [27,67], the traits that we assessed can help us better understand how resistance alleles could spread in parasitic nematode populations.

Our competitive fitness and development assay results confirm previous findings, which showed that a loss of *ben-1* confers albendazole resistance and that loss of both *avr-14* and *avr-15* or a loss of all three GluCl subunits are necessary to confer ivermectin resistance [39,43,44,49,58,60]. However, animals with the loss of both *avr-14* and *avr-15* or the loss of all three GluCl subunits did not significantly differ in ivermectin response as previously reported in mutagenesis studies [60]. It is also critical to note that strains with a loss of both *avr-14* and *avr-15* or a loss of all three GluCl subunits have significant fitness consequences when not under ivermectin exposure, rendering it unlikely that loss-of-function mutations will occur in these genes and confer ivermectin resistance in nature.

Prior to this study, minimal research had been performed to assess the quantitative contributions of GluCl subunits on nematode fitness. To identify why GluCls in parasites lack variation, we tested the contributions of three genes that encode GluCl subunits on *C. elegans* fitness. We found that a loss of *avr-14* alone or in combination with *glc-1* has significant fitness consequences in ivermectin but not when in albendazole or control conditions. Overall, a loss of *avr-15* has profoundly detrimental effects compared to the control strain across all conditions. An animal with a loss of *avr-15* in combination with *avr-14* must remain under constant ivermectin pressure to exhibit any fitness benefit compared to the control strain. Finally, a loss of *glc-1* does

bioRxiv preprint doi: https://doi.org/10.1101/2024.02.01.578300; this version posted February 6, 2024. The copyright holder for this preprint (which was not certified by peer review) is the author/funder, who has granted bioRxiv a license to display the preprint in perpetuity. It is made available under aCC-BY-NC 4.0 International license.

not affect fitness across conditions, indicating perhaps why natural mutations of this gene are found in *C. elegans* wild populations [41,68,69]. Our investigation did not reveal any indication that *glc-1* is responsible for conferring resistance to ivermectin, which contradicts earlier findings [68,69]. Previous studies focused on different phenotypic traits such as body bends, paralysis, and gene expression, used different genetic approaches to assess resistance, and measured nematode response against different macrocyclic lactones than what was tested here. The discrepancy between our findings and earlier research underscores the necessity of evaluating multiple traits, as the response to anthelmintic treatment can vary depending on the trait measured.

Several reasons might explain the infrequent detection of GluCl subunits mutated in parasitic nematode isolates that have ivermectin resistance, including variation in GluCl gene family number, interactions between genes outside the GluCl family, poor nematode genome quality, and the locations of GluCl tissue expression. First, we do not fully understand the composition of GluCls. The GluCls are members of the pentameric ligand-gated ion channel family and, similar to other members of this family, the functional channels formed *in vivo* could be homomeric or heteromeric [62]. More research needs to be done to elucidate the subunit composition of GluCls across parasitic nematode species. In addition, no auxiliary proteins, analogous to the genes that influence the trafficking and assembly of nematode nicotinic acetylcholine receptors, have been reported for the GluCls, and we do not know if any such proteins exist [62]. Furthermore, although *avr-14*, *avr-15*, *glc-1*, *glc-2*, *glc-3*, and *glc-4* are predicted to be conserved widely across nematode species [70], *avr-14* is currently the only GluCl gene found to be highly conserved throughout *Nematoda* [55]. A polymorphism in an *avr-14* ortholog has been identified in *Cooperia oncophora*, and polymorphisms in several genes (*glc-3* and *glc-5*) have been identified in resistant isolates of *Haemonchus contortus [22,71–73]*. Importantly, these results are correlative and do not show a causal connection between ivermectin resistance and GluCl genes. Additionally, research in both *C. elegans* and parasitic nematodes

bioRxiv preprint doi: https://doi.org/10.1101/2024.02.01.578300; this version posted February 6, 2024. The copyright holder for this preprint (which was not certified by peer review) is the author/funder, who has granted bioRxiv a license to display the preprint in perpetuity. It is made available under aCC-BY-NC 4.0 International license.

455 has led to the suggestion that ivermectin resistance might be polygenic [62], so combinations of
456 genes must also be considered.

457 Second, a lack of variation in GluCl genes in ivermectin-resistant parasites has led
458 researchers to search for additional genes outside this gene family involved in the MoR of
459 ivermectin. It is unknown why, despite GluCls being understood as the MoA and confirmation of
460 association with resistance to ivermectin in *C. elegans*, the GluCl subunits have not been widely
461 associated with resistance in parasite populations. As illustrated here, the fitness disadvantages
462 of losing *avr-14* or *avr-15* alone or in combination outweigh any ivermectin resistance.
463 Additionally, the loss of *glc-1* alone or in combination with *avr-14* or *avr-15* had no discernible
464 impact on fitness across conditions but also did not confer ivermectin resistance. Our findings
465 provide insights into why GluCls have not been clearly associated with resistance in parasites.

466 To date, ivermectin resistance across *Nematoda* appears to involve various genes and
467 mechanisms [74]. Additional genes outside of those that encode for GluCl subunits are implicated
468 in the MoR of ivermectin, which includes Dyf genes and genes involved in neuronal development
469 and function, such as *unc-7*, *unc-9*, *unc-38*, and *unc-63* [60,75]. Genes involved in ivermectin
470 metabolism, such as ATP-binding cassette (ABC) transporters, cytochrome P450 enzymes,
471 GABA receptors, and other signaling proteins, have been implicated in ivermectin resistance
472 though much more research needs to be done to determine their role in the MoR of ivermectin
473 [62,76,77]. Ivermectin also affects some nicotinic receptors and acts as a positive allosteric
474 modulator of the α7 neuronal nicotinic acetylcholine receptor [78]. Overall, additional genes
475 outside of the GluCl family could be involved in the MoR of ivermectin, and more research is
476 needed to determine the role that each gene plays in ivermectin resistance.

477 Third, it is important to highlight that GluCl subunits have been well characterized in only
478 a few nematode species, partly because of poor-quality genomes. Recent efforts have been made
479 to generate high-quality reference parasitic nematode genomes [79–82]. WormBase Parasite
480 [83,84] serves as the main repository for these data, which now hosts a collection of 240

bioRxiv preprint doi: https://doi.org/10.1101/2024.02.01.578300; this version posted February 6, 2024. The copyright holder for this preprint (which was not certified by peer review) is the author/funder, who has granted bioRxiv a license to display the preprint in perpetuity. It is made available under aCC-BY-NC 4.0 International license.

genomes, representing 181 species. Recently, 864 total GluCl gene predictions were categorized across 125 species into orthologous groups, which suggests that there are additional GluCl subunits across *Nematoda* that have yet to be discovered [70]. As our genome assemblies, technologies, and analytical techniques improve, so will our ability to search for and identify GluCl genes.

Fourth, although albendazole and ivermectin target different genes and have different MoR, it is conceivable that the genes targeted by both drugs can be expressed in the same tissues or cells. To date, our understanding of the MoR and tissue-specific susceptibility for most anthelmintic drugs across nematode species is not well known. Previous research has shown that *ben-1* is highly expressed in cholinergic neurons, which causes BZ susceptibility [42]. However, analogous experiments are imperative to ascertain in which tissues GluCl subunit genes underlie ivermectin susceptibility. Expression data from the Complete Gene Expression Map of the *C. elegans* Nervous System (CeNGEN) [85] shows an overlap in *ben-1* and GluCl subunit gene expression in neurons (**S8 Fig**). In particular, a pronounced overlap between *ben-1* and *avr-14* expression in cholinergic neurons is observed, which suggests albendazole and ivermectin could target the same tissues. The overlap in expression in the same neurotransmitters between *ben-1* and the GluCl subunits could explain the small advantages that *ben-1* conferred in ivermectin and the GluCls in albendazole in the HTA (**Fig 4**). The co-expression of two genes in the same neurons implies a potential functional relationship between the genes, which could collaborate to regulate specific neural functions associated with the neurotransmitter. A shared expression between genes could lead to unexpected consequences, such as changes in sensitivity to other drugs or alterations in neural processes beyond resistance to the targeted drug. Given that multiple GluCls are present in *C. elegans*, a redundancy in function is conceivable. As neurotransmitters play essential roles in physiological processes, including behavior, locomotion, and sensory perception, it is imperative to delineate which neurons are implicated in GluCl expression and consequently influences ivermectin susceptibility. Fully understanding the MoR

bioRxiv preprint doi: https://doi.org/10.1101/2024.02.01.578300; this version posted February 6, 2024. The copyright holder for this preprint (which was not certified by peer review) is the author/funder, who has granted bioRxiv a license to display the preprint in perpetuity. It is made available under aCC-BY-NC 4.0 International license.

of each drug class is complicated by the implication that genes associated with drug resistance overlap in expression within the same neuronal pathways. Finally, it is important to note that all the expression data discussed here have been performed in *C. elegans* and not parasitic nematode models, so differences among nematodes might not be captured entirely by research on this free-living nematode species.

In summary, our experiments suggest that loss of *ben-1* confers albendazole resistance and that multiple mutations in GluCl genes are required to obtain ivermectin resistance. Nevertheless, our understanding of ivermectin's MoR remains incomplete because we have not identified all the genes involved in ivermectin resistance. To solve this problem, we need to conduct additional experiments that quantitatively assess the fitness effects of all six GluCl subunit genes singly and in combination, both in control and ivermectin conditions. Moreover, to identify in which tissues GluCl function underlies ivermectin susceptibility, transgenic strains that express each GluCl subunit genes in different tissues will determine the tissue-specific susceptibility of ivermectin. Finally, when considering the opportunity for multi-drug resistance to occur, either by cross-resistance or independent selection, our data suggest that cross-resistance is unlikely because *ben-1* and the GluCl subunits do not appear to target the same MoR in *C. elegans*.

MATERIALS AND METHODS

Generation of *ben-1* and GluCl deletion strains

Nine *Caenorhabditis elegans* deletion strains generated from the N2 background were used in this study (**Table S1**). The *avr-14*, *avr-15*, and *glc-1* single deletion mutant strains were generated in the PD1074 background using CRISPR-Cas9 genome editing by SunyBiotech (Fujian, China). The PD1074 strain is a lineal descendent of the laboratory-adapted N2 Bristol strain. The double and triple GluCl deletion mutant strains were generated by crossing the single GluCl deletion strains.

bioRxiv preprint doi: https://doi.org/10.1101/2024.02.01.578300; this version posted February 6, 2024. The copyright holder for this preprint (which was not certified by peer review) is the author/funder, who has granted bioRxiv a license to display the preprint in perpetuity. It is made available under aCC-BY-NC 4.0 International license.

C. elegans strains and maintenance

In the competitive fitness assays, the barcoded wild-type strain PTM229 *dpy-10* (*kah81*) was used as a control strain. The PTM229 strain is an N2 strain that contains a synonymous change in the *dpy-10* locus that does not have any growth effects compared to the normal laboratory N2 strain [65]. Animals were maintained at 20ºC on 6 cm plates with modified nematode growth medium (NGMA), which contains 1% agar and 0.7% agarose to prevent animals from burrowing. The NGMA plates were seeded with the *Escherichia coli* strain OP50 as a nematode food source. All strains were grown for three generations without starvation on NGMA plates before anthelmintic exposure to reduce the transgenerational effects of starvation stress. The specific growth conditions for nematodes used in each assay are described below.

Nematode food preparation for NGMA assays

A batch of OP50 *E. coli* was grown and used as a nematode food source for each competitive fitness and fecundity assay. A frozen stock of OP50 *E. coli* was streaked onto a 10 cm Luria-Bertani (LB) agar plate and incubated overnight at 37ºC. The following day, a single bacterial colony was transferred into two culture tubes that contained 5 ml of 1x LB. The starter cultures and two negative controls (1X LB without *E. coli*) were incubated for 18 hours at 37ºC shaking at 210 rpm. The OD_{600} value of the starter cultures were measured using a spectrophotometer (BioRad, SmartSpec Plus) to calculate how much starter culture was needed to inoculate a one-liter culture at an OD_{600} value of 0.005. For each assay, one culture contained one liter of pre-warmed 1X LB inoculated with the starter culture that grew for approximately 4 - 4.5 hours at 37ºC at 210 rpm. Cultures were grown until they reached an OD_{600} value between 0.45 and 0.6. Cultures were transferred to 4ºC to suspend growth. OP50 was spotted on NGMA test plates (two per culture) and grown at 37ºC overnight to ensure a normal lawn was grown with no contamination.

Nematode food preparation for liquid culture assays

bioRxiv preprint doi: https://doi.org/10.1101/2024.02.01.578300; this version posted February 6, 2024. The copyright holder for this preprint (which was not certified by peer review) is the author/funder, who has granted bioRxiv a license to display the preprint in perpetuity. It is made available under aCC-BY-NC 4.0 International license.

One batch of HB101 *E. coli* was used as a nematode food source for all HTAs. A frozen stock of HB101 *E. coli* was streaked onto a 10 cm Luria-Bertani (LB) agar plate and incubated overnight at 37ºC. The following day, a single bacterial colony was transferred into three culture tubes that contained 5 ml of 1x Horvitz Super Broth (HSB). The starter cultures and two negative controls (1X HSB without *E. coli*) were incubated for 18 hours at 37ºC shaking at 180 rpm. The OD_{600} value of the starter cultures were measured using a spectrophotometer (BioRad, SmartSpec Plus) to calculate how much starter culture was needed to inoculate a one-liter culture at an OD_{600} value of 0.001. A total of 14 cultures each of which contained one liter of pre-warmed 1X HSB inoculated with the starter culture grew for 15 hours at 37ºC while shaking at 180 rpm until cultures were in the late log growth phase. After 15 hours, flasks were removed from the incubator and transferred to 4ºC to arrest growth. The 1X HSB was removed from the cultures through three rounds of washing and centrifugation, where the supernatant was removed, and the bacterial cells were pelleted. Bacterial cells were washed, resuspended in K medium, pooled, and transferred to a 2 L glass beaker. The OD_{600} value of the bacterial suspension was measured and diluted to a final concentration of OD_{600}100 with K medium, aliquoted to 15 ml conicals, and stored at -80ºC for use in the HTAs.

Anthelmintic stock preparation

Albendazole and ivermectin stock solutions were prepared with dimethyl sulfoxide (DMSO) (Fisher Scientific, Catalog # D1281). Albendazole (Sigma-Aldrich, Catalog # A4673-10G) was used at a concentration of 1.25 µM in the competitive fitness and brood size assays and 30 µM in the HTA. Ivermectin (Sigma-Aldrich, Catalog # I8898-1G) was used at a concentration of 1.5 nM in the competitive fitness and brood size assays and 250 nM and 500 nM in the HTA. Anthelmintic stock solutions were prepared, aliquoted, and stored at -20ºC for use in the assays (**Table S4**). Anthelmintic stock concentrations, companies, and details for the wild strain HTA are documented in *Methods*, *Wild Strain HTA and Spearman rank-order correlations.*

Competitive fitness assays

bioRxiv preprint doi: https://doi.org/10.1101/2024.02.01.578300; this version posted February 6, 2024. The copyright holder for this preprint (which was not certified by peer review) is the author/funder, who has granted bioRxiv a license to display the preprint in perpetuity. It is made available under aCC-BY-NC 4.0 International license.

We used previously established pairwise competitive fitness assays to assess nematode fitness [28,65]. The fitness of a strain was determined by comparing the allele frequency of a test strain against the allele frequency of the wild-type control strain PTM229. Strains contain molecular barcodes to distinguish between the two strains using oligonucleotide probes complementary to each barcoded allele. Ten L4 larval individuals of each strain were placed onto a single 6 cm NGMA plate along with ten L4 larval individuals of the PTM229 strain. Ten independent NGMA plates of each competition were prepared for each strain in each condition: control (DMSO), albendazole (1.25 µM), or ivermectin (1.5 nM). The N2 strain was included to ensure that assays were reproducible and that all plates had effective albendazole and ivermectin concentrations. Plates were grown for roughly one week to starvation. Animals were transferred to a new NGMA plate of the same condition by the transfer of a 0.5 cm^3 NGMA piece from the starved plate onto the new plate. The remaining individuals on the starved plate were washed into a 15 mL Falcon™ tube with M9 buffer, concentrated by centrifugation, transferred to 1.5 mL Eppendorf tubes, and stored at -80°C. Competitions were performed for seven generations, and animals were collected after generations one, three, five, and seven. DNA was extracted in randomized blocks using the DNeasy Blood & Tissue kit (Qiagen, Catalog # 69506), purified with the Zymo DNA cleanup kit (Catalog # D4064), and diluted to approximately 1 ng/µL.

We quantified the relative allele frequency of each strain as previously described [28,65]. A droplet digital PCR (ddPCR) approach with TaqMan probes (Applied Biosciences) was used. Using TaqMan probes, the ddPCR assay was performed with a Bio-Rad QX200 device with standard probe absolute quantification settings. The TaqMan probes selectively bind to wild-type *dpy-10* and the *dpy-10* allele present in PTM229 [65]. Thresholds were manually selected and set in QX Manager software (Version 2.1). Relative allele frequencies of each tested allele were calculated using the QuantaSoft software. Calculations of relative fitness were calculated by linear regression analysis to fit the data to a one-locus generic selection model [65] (**Table S5, Table S6**).

bioRxiv preprint doi: https://doi.org/10.1101/2024.02.01.578300; this version posted February 6, 2024. The copyright holder for this preprint (which was not certified by peer review) is the author/funder, who has granted bioRxiv a license to display the preprint in perpetuity. It is made available under aCC-BY-NC 4.0 International license.

610 **Brood size assays**

611 Brood size assays were used to assess nematode fecundity for the laboratory-adapted
612 strain, N2, and the eight mutant strains. Prior to each assay, strains were grown for three
613 generations at 20°C to reduce cross-generational effects. For each *C. elegans* strain in the fourth
614 generation, single L4 larval stage hermaphrodites were picked to each of ten 6 cm NGMA plates
615 spotted with OP50 and were maintained at 20°C. Ten independent 6 cm NGMA plates seeded
616 with *E. coli* OP50 were prepared for each strain in each condition, control (DMSO), albendazole
617 (1.25 μM), and ivermectin (1.5 nM) and maintained at 20°C. For each assay plate, the original
618 hermaphrodite parent was transferred to a fresh plate every 24 hours for 96 hours. A custom-built
619 imaging platform (DMK 23GP031 camera; Imaging Source, Charlotte, NC, USA) was used to
620 collect images for each of the first four assay plates (0, 24, 48, and 72-hour assay plates) 48
621 hours after the removal of the parent from each NGMA plate. Images of the fifth assay plates
622 were collected 72 hours after the final transfer of the parents. The total offspring were counted
623 from each image by visual inspection using the use of the Multi-point tool in ImageJ (Version
624 1.54f) [86]. The original hermaphrodite parents were excluded from the counts. The number of
625 offspring in each of the first four assay plates corresponds to the daily fecundity (**S3 Fig, S4 Fig,**
626 **S5 Fig**) The number of offspring on the fifth assay plates contained offspring from three days
627 (days 5-7). For each biological replicate of each *C. elegans* strain, the lifetime fecundity was
628 calculated as the total number of offspring from the five plates (**Fig 3**). Replicates where the
629 original hermaphrodite parent died were excluded from the analysis of lifetime fecundity. Only
630 biological replicates with data from all five assay plates were used to calculate daily and total
631 fecundity (**Table S7**). Daily intrinsic growth rate (r) for each strain was calculated by $r = ln(mx)/x$,
632 where x is animal age after hatching (2 + day of adulthood), and m_x is cumulative fecundity by
633 each age [66,87,88].

634 **High-throughput assays (HTAs)**

bioRxiv preprint doi: https://doi.org/10.1101/2024.02.01.578300; this version posted February 6, 2024. The copyright holder for this preprint (which was not certified by peer review) is the author/funder, who has granted bioRxiv a license to display the preprint in perpetuity. It is made available under aCC-BY-NC 4.0 International license.

Populations of each strain were amplified and bleach-synchronized for three independent assays. Independent bleach synchronizations controlled for variation in embryo survival and subsequent effects on developmental rates that could be attributed to bleach effects. After bleach synchronization, approximately 30 embryos were dispensed into the wells of a 96-well microplate in 50 µL of K medium. One 96-well plate was prepared per bleach for each strain. Each 96-well microplate was prepared, labeled, and sealed using gas-permeable sealing films (Fisher Scientific, Catalog # 14-222-043). Plates were placed in humidity chambers to incubate overnight at 20ºC while shaking at 170 rpm (INFORS HT Multitron shaker). The following morning, food was prepared to feed the developmentally arrested first larval stage animals (L1s) using the required number of OD_{600}100 HB101 aliquots (see *Nematode food preparation for liquid culture assays*). The aliquots were thawed at room temperature, combined into a single conical tube, and diluted to an OD_{600}30 with K medium. To inhibit further bacterial growth and prevent contamination, 150 µM of kanamycin was added to the HB101. Working with a single drug at a time, an aliquot of anthelmintic stock solution was thawed at room temperature (see *Anthelmintic stock preparation*) and diluted to a working concentration. The anthelmintic working concentration was set to the concentration that would give the highest desired dose when added to the 96-well microplates at 1% of the total well volume. The dilution of the anthelmintic working solution was prepared using the same diluent, DMSO, used to make the stock solution. The anthelmintic dilution was then added to an aliquot of the OD_{600}30 K medium at a 3% volume/volume ratio. Next, 25 µl of the food and anthelmintic mixture was transferred into the appropriate wells of the 96-well microplates to feed the arrested L1s at a final HB101 concentration of OD_{600}10 and expose L1 larvae to the given anthelmintic. Immediately afterward, the 96-well microplates were sealed using a new gas permeable sealing film, returned to the humidity chambers, and incubated for 48 hours at 20ºC shaking at 170 rpm. The remaining 96-well microplates were fed and exposed to anthelmintics in the same manner. After 48 hours of incubation in the presence of food and anthelmintic, the 96-well microplates were removed from the incubator and treated with 50 mM

bioRxiv preprint doi: https://doi.org/10.1101/2024.02.01.578300; this version posted February 6, 2024. The copyright holder for this preprint (which was not certified by peer review) is the author/funder, who has granted bioRxiv a license to display the preprint in perpetuity. It is made available under aCC-BY-NC 4.0 International license.

sodium azide in M9 for 10 minutes to paralyze and straighten nematodes. Images of nematodes in the microplates were immediately captured using a Molecular Devices ImageXpress Nano microscope (Molecular Devices, San Jose, CA) using a 2X objective. The ImageXpress Nano microscope acquires brightfield images using a 4.7 megapixel CMOS camera and stores images in a 16-bit TIFF format. The images were used to quantify the development of nematodes in the presence of anthelmintics as described below (see *High-throughput imager assay [HTA] data collection* and *data cleaning*).

High-throughput assay (HTA) data collection and data cleaning

The CellProfiler software program (Version 4.0.3) was used to characterize and quantify biological data from the image-based assays. Custom software packages designed to extract animal measurements from images collected on the Molecular Devices ImageXpress Nano microscope were previously described [89]. CellProfiler modules and Worm Toolbox were developed to extract morphological features of individual *C. elegans* animals from images from the HTA [90]. Worm model estimates and custom CellProfiler pipelines were written using the WormToolbox in the GUI-based instance of CellProfiler [91]. Next, a Nextflow pipeline (Version 20.01.0) was written to run command-line instances of CellProfiler in parallel on the Quest High-Performance Computing Cluster (Northwestern University). The CellProfiler workflow can be found at (https://github.com/AndersenLab/cellprofiler-nf). The custom CellProfiler pipeline generates animal measurements by using four worm models: three worm models tailored to capture animals at the L4 larval stage, in the L2 and L3 larval stages, and the L1 larval stage, respectively, as well as a “multi-drug high dose” (MDHD) model, to capture animals with more abnormal body sizes caused by extreme anthelmintic responses. These measurements composed our raw dataset.

Data analysis steps have been modified from previous reports [37,92]. All analyses were performed using the R statistical environment (version 4.2.1) unless stated otherwise. The HTA produced hundreds of images per experimental block; thus, we implemented a systematic

bioRxiv preprint doi: https://doi.org/10.1101/2024.02.01.578300; this version posted February 6, 2024. The copyright holder for this preprint (which was not certified by peer review) is the author/funder, who has granted bioRxiv a license to display the preprint in perpetuity. It is made available under aCC-BY-NC 4.0 International license.

687 approach to assess the quality of animal measurement data in each well. Several steps were
688 implemented to clean the raw image data using metrics indicative of high-quality animal
689 measurements for downstream analysis.

690 1) Objects with a *Worm_Length* > 30 pixels, 100 microns, were removed from the
691 CellProfiler data to (A) retain L1 and MDHD-sized animals and (B) remove
692 unwanted particles [93]. By using the *Worm_Length* > 30 pixels threshold to retain
693 small sensitive animals, more small objects, such as debris, were also retained
694 [37].
695 2) R/*easyXpress* [89] was used to filter measurements from worm objects within
696 individual wells with statistical outliers and to parse measurements from multiple
697 worm models down to single measurements for single animals.
698 3) The data were visualized by drug, drug concentration, assay, strain, and worm
699 model for two purposes. First, to ensure that each drug, by assay, contained
700 control wells that had a *mean_wormlength_um* between 600 - 800 µm, the size of
701 an L4 animal. If the *mean_wormlength_um* in the control wells was not between
702 the 600 - 800 µm range, then that strain and/or assay were removed for the drug.
703 This filter ensured the control, DMSO, wells primarily contained L4 animals.
704 Second, we wanted to identify drugs that contained a high abundance of MDHD
705 model objects across all assays and drug concentrations. Drugs with an
706 abundance of objects classified by the MDHD model across assays and
707 concentrations likely contain debris. We then reduced the data to wells that
708 contained between five and thirty animals, under the null hypothesis that the
709 number of animals is an approximation of the expected number of embryos
710 originally titered into wells (approximately 30). Given that our analysis relied on
711 well median animal length measurements, we excluded wells with less than five
712 animals to reduce sampling error.

bioRxiv preprint doi: https://doi.org/10.1101/2024.02.01.578300; this version posted February 6, 2024. The copyright holder for this preprint (which was not certified by peer review) is the author/funder, who has granted bioRxiv a license to display the preprint in perpetuity. It is made available under aCC-BY-NC 4.0 International license.

4) Next, we removed measurements from each anthelmintic drug that were no longer represented in at least 80% of the independent assays because of previous data filtering steps or had fewer than five measurements per strain.

5) Finally, we normalized the data by (1) regressing variation attributable to assay and technical replicate effects and (2) normalizing these extracted residual values to the average control phenotype. For each anthelmintic drug, we estimated a linear model using the raw phenotype measurement as the response variable and both assay and technical replicate identity as explanatory variables following the formula *median_wormlength_um ~ Metadata_Experiment + bleach* using the *lm()* function in base R. We then extracted the residuals from the linear model for each anthelmintic and subtracted normalized phenotype measurements in each anthelmintic from the mean normalized phenotype in control conditions. These normalized phenotype measurements were used in all downstream statistical analyses.

Wild Strain HTA and Spearman rank-order correlations

Populations of 124 *C. elegans* wild strains were processed using the HTA as described above (see *High-throughput assays [HTAs]*). Each wild strain was exposed to the following benzimidazoles or macrocyclic lactones at the denoted concentrations: abamectin (2 nM) (Millipore sigma, Catalog # 31732), albendazole (10.65 µM) (Fluka, Catalog # A4673-10G), benomyl (20.66 µM) (Sigma Aldrich, Catalog # 45339-250MG), doramectin (5 nM) (Millipore Sigma, Catalog # 33993), eprinomectin (44 nM) (Millipore Sigma, Catalog # 32526), ivermectin (12 nM) (Sigma-Aldrich, Catalog # I8898-1G), fenbendazole (10.65 µM) (Sigma-Aldrich, Catalog # F5396-5G), mebendazole (48 µM) (Sigma-Aldrich, Catalog # M2523-25G), milbemycin oxime (120 nM) (Millipore Sigma, Catalog # 1443806), moxidectin (3 nM) (Millipore Sigma, Catalog # 113507-06-5), ricobendazole (25 µM) (Santa Cruz Biotechnology, Catalog # sc-205838), selamectin (0.39 µM) (Sigma-Aldrich, Catalog # SML2663-25MG), and thiabendazole (62.99 µM)

bioRxiv preprint doi: https://doi.org/10.1101/2024.02.01.578300; this version posted February 6, 2024. The copyright holder for this preprint (which was not certified by peer review) is the author/funder, who has granted bioRxiv a license to display the preprint in perpetuity. It is made available under aCC-BY-NC 4.0 International license.

(Sigma-Aldrich, Catalog # T5535-50G) using the methods as described in *High-throughput assays (HTAs)*. After measuring nematode responses, phenotypic data were cleaned and processed as described in *High-throughput assay (HTA) data collection and data cleaning***.** Wild strains that lacked phenotype measurements for one or more drugs were removed from the dataset prior to statistical analysis.

Spearman rank-order correlation and significance testing were performed using the R package *Hmisc* (version 4.1.1). Subsequently, hierarchical clustering was performed using the R package *pheatmap* (version 1.0.12). Significant correlations ($p < 0.05$) were recorded (**Table S3)**. The resulting heat map and dendrogram (**Fig 5**) were constructed using Euclidean distance and complete linkage metrics, and split into their two largest clusters.

Neuronal expression patterns of genes encoding GluCls and beta-tubulin

Single-cell RNA-sequencing data were obtained from the Complete Gene Expression Map of the *C. elegans* Nervous System (CeNGEN) [85]. Using the CeNGEN scRNA-seq dataset, gene expression for each of the genes of interest was extracted from the database with a threshold of 2 (**Table S8)**. All expression values are in transcripts per million (TPM) [94]. All data collection, processing, normalization, and analysis of the CeNGEN data can be found at https://www.cengen.org/.

Gene models for *ben-1* and the three genes encoding for GluCl subunits

Gene models of *ben-1*, *avr-14*, *avr-15*, and *glc-1* were created with a modified script retrieved from the Gene Model Visualization Kit (https://github.com/AndersenLab/GMVK). Gene models physical positions were extracted from WormBase (WS283) [95]. The location of each gene deletion is denoted beneath each gene model.

Data availability

All code and data used to replicate the data analysis and figures are available on GitHub at https://github.com/AndersenLab/bzml_manuscript. Table S1 contains the list of strains and genotypes, along with primer and guide RNA sequences. Table S2 contains all the data used to

bioRxiv preprint doi: https://doi.org/10.1101/2024.02.01.578300; this version posted February 6, 2024. The copyright holder for this preprint (which was not certified by peer review) is the author/funder, who has granted bioRxiv a license to display the preprint in perpetuity. It is made available under aCC-BY-NC 4.0 International license.

765 analyze the HTAs. Table S3 contains the *p*-values from the correlation matrices. Table S4
766 contains all the anthelmintic drugs and concentrations used along with the manufacturer's details.
767 Table S5 contains the competitive fitness assay data for DMSO and albendazole. Table S6
768 contains the competitive fitness assay data for DMSO and ivermectin. Table S7 contains the
769 results from the fecundity assays. Table S8 contains the list of cell types expressing beta-tubulin
770 and GluCl subunit genes from CeNGEN.
771

772 **SUPPORTING INFORMATON**

773 **Table S1.** A list of strains and genotypes, along with primer and guide RNA sequences
774
775 **Table S2.** High-throughput assay (HTA) data

776 **Table S3.** *p*-values from correlation matrices

777 **Table S4.** Anthelmintic drugs, concentrations used, and manufacturer's details

778 **Table S5**. Competitive fitness assay data for DMSO and albendazole

779 **Table S6**. Competitive fitness assay data for DMSO and ivermectin

780 **Table S7.** Fecundity data

781 **Table S8.** Cell types expressing beta-tubulin and GluCl subunit genes from CeNGEN
782

783 **AUTHOR CONTRIBUTIONS**

784 **Conceptualization:** Erik C. Andersen

785 **Data Curation:** Amanda O. Shaver

786 **Formal Analysis:** Amanda O. Shaver

787 **Funding Acquisition:** Erik C. Andersen

788 **Investigation:** Amanda O. Shaver

789 **Methodology:** Amanda O. Shaver, Isabella R. Miller, Etta S. Schaye, Nicolas D. Moya, James
790 Bryant Collins, Janneke Wit, Alyssa H. Blanco, Fiona M. Shao, Elliot J. Andersen, Gracie
791 Paredes, Sharik A. Khan

bioRxiv preprint doi: https://doi.org/10.1101/2024.02.01.578300; this version posted February 6, 2024. The copyright holder for this preprint (which was not certified by peer review) is the author/funder, who has granted bioRxiv a license to display the preprint in perpetuity. It is made available under aCC-BY-NC 4.0 International license.

Project Administration: Erik C. Andersen

Resources: Erik C. Andersen

Software: Amanda O. Shaver

Supervision: Erik C. Andersen

Validation: Amanda O. Shaver

Visualization: Amanda O. Shaver, Etta S. Schaye, Nicolas D. Moya

Writing - Original Draft Preparation: Amanda O. Shaver

Writing - Review & Editing: Amanda O. Shaver, Erik C. Andersen, Isabella R. Miller, Etta S. Schaye, Nicolas D. Moya, James Bryant Collins

ACKNOWLEDGMENTS

We would like to thank members of the Andersen laboratory for their feedback and helpful comments on this manuscript. This study was supported by the National Institutes of Health NIAID grant R01AI153088 to ECA. We thank SunyBiotech for providing us with the single GluCl deletion strains. We thank the *Caenorhabditis* Natural Diversity Resource (NSF Capacity grant 2224885) for providing us with strains used in the wild strain HTA. We thank Joy N. Nyaanga, Timothy A. Crombie, and Samuel J. Widmayer for creating *easyXpress*.

COMPETING INTERESTS

The authors have declared that no competing interests exist

bioRxiv preprint doi: https://doi.org/10.1101/2024.02.01.578300; this version posted February 6, 2024. The copyright holder for this preprint (which was not certified by peer review) is the author/funder, who has granted bioRxiv a license to display the preprint in perpetuity. It is made available under aCC-BY-NC 4.0 International license.

REFERENCES

1. Organization WH, Others. Global Health Estimates 2020: Disease burden by Cause, Age, Sex, by Country and by Region, 2000-2019. WHO; 2020. 2021.

2. Dieterich, Sommer. How to become a parasite–lessons from the genomes of nematodes. Trends Genet. Available: https://www.sciencedirect.com/science/article/pii/S016895250900064X

3. Parkinson J, Mitreva M, Whitton C, Thomson M, Daub J, Martin J, et al. A transcriptomic analysis of the phylum Nematoda. Nat Genet. 2004;36: 1259–1267.

4. Osei-Atweneboana MY, Eng JK, Boakye DA, Gyapong JO, Prichard RK. Prevalence and intensity of Onchocerca volvulus infection and efficacy of ivermectin in endemic communities in Ghana: a two-phase epidemiological study. Lancet. 2007;369: 2021–2029.

5. Awadzi K, Attah SK, Addy ET, Opoku NO, Quartey BT, Lazdins-Helds JK, et al. Thirty-month follow-up of sub-optimal responders to multiple treatments with ivermectin, in two onchocerciasis-endemic foci in Ghana. Ann Trop Med Parasitol. 2004;98: 359–370.

6. Albonico M, Ramsan M, Wright V, Jape K, Haji HJ, Taylor M, et al. Soil-transmitted nematode infections and mebendazole treatment in Mafia Island schoolchildren. Ann Trop Med Parasitol. 2002;96: 717–726.

7. De Clercq D, Sacko M, Behnke J, Gilbert F, Dorny P, Vercruysse J. Failure of mebendazole in treatment of human hookworm infections in the southern region of Mali. Am J Trop Med Hyg. 1997;57: 25–30.

8. Eberhard ML, Lowrie RC Jr, Lammie PJ. Persistence of microfilaremia in bancroftian filariasis after diethylcarbamazine citrate therapy. Trop Med Parasitol. 1988;39: 128–130.

9. Kotze AC, Gilleard JS, Doyle SR, Prichard RK. Challenges and opportunities for the adoption of molecular diagnostics for anthelmintic resistance. Int J Forecast. 2020. Available: https://www.sciencedirect.com/science/article/pii/S2211320720300476

10. Sutherland IA, Leathwick DM. Anthelmintic resistance in nematode parasites of cattle: a global issue? Trends Parasitol. 2011;27: 176–181.

11. Besier B. New anthelmintics for livestock: the time is right. Trends Parasitol. 2007;23: 21–24.

12. Wolstenholme AJ, Fairweather I, Prichard R, von Samson-Himmelstjerna G, Sangster NC. Drug resistance in veterinary helminths. Trends Parasitol. 2004;20: 469–476.

13. Leathwick DM, Hosking BC, Bisset SA, McKay CH. Managing anthelmintic resistance: is it feasible in New Zealand to delay the emergence of resistance to a new anthelmintic class? N Z Vet J. 2009;57: 181–192.

14. Kaplan RM. Biology, Epidemiology, Diagnosis, and Management of Anthelmintic Resistance in Gastrointestinal Nematodes of Livestock. Vet Clin North Am Food Anim Pract. 2020;36: 17–30.

15. Sargison ND, Jackson F, Bartley DJ, Wilson DJ, Stenhouse LJ, Penny CD. Observations

bioRxiv preprint doi: https://doi.org/10.1101/2024.02.01.578300; this version posted February 6, 2024. The copyright holder for this preprint (which was not certified by peer review) is the author/funder, who has granted bioRxiv a license to display the preprint in perpetuity. It is made available under aCC-BY-NC 4.0 International license.

on the emergence of multiple anthelmintic resistance in sheep flocks in the south-east of Scotland. Vet Parasitol. 2007;145: 65–76.

16. Sutherland IA, Brown AE, Leathwick DM. Selection for drug-resistant nematodes during and following extended exposure to anthelmintic. Parasitology. 2000;121 (Pt 2): 217–226.

17. Fissiha W, Kinde MZ. Anthelmintic Resistance and Its Mechanism: A Review. Infect Drug Resist. 2021;14: 5403–5410.

18. Janssen IJI, Krücken J, Demeler J, Basiaga M, Kornaś S, von Samson-Himmelstjerna G. Genetic variants and increased expression of Parascaris equorum P-glycoprotein-11 in populations with decreased ivermectin susceptibility. PLoS One. 2013;8: e61635.

19. Kaplan RM. Drug resistance in nematodes of veterinary importance: a status report. Trends Parasitol. 2004;20: 477–481.

20. Blaxter ML, De Ley P, Garey JR, Liu LX, Scheldeman P, Vierstraete A, et al. A molecular evolutionary framework for the phylum Nematoda. Nature. 1998;392: 71–75.

21. Kaplan RM, Vidyashankar AN. An inconvenient truth: global worming and anthelmintic resistance. Vet Parasitol. 2012;186: 70–78.

22. Beech RN, Skuce P, Bartley DJ, Martin RJ, Prichard RK, Gilleard JS. Anthelmintic resistance: markers for resistance, or susceptibility? Parasitology. 2011;138: 160–174.

23. Beach MJ, Streit TG, Addiss DG, Prospere R, Roberts JM, Lammie PJ. Assessment of combined ivermectin and albendazole for treatment of intestinal helminth and Wuchereria bancrofti infections in Haitian schoolchildren. Am J Trop Med Hyg. 1999;60: 479–486.

24. Patel C, Hürlimann E, Keller L, Hattendorf J, Sayasone S, Ali SM, et al. Efficacy and safety of ivermectin and albendazole co-administration in school-aged children and adults infected with Trichuris trichiura: study protocol for a multi-country randomized controlled double-blind trial. BMC Infect Dis. 2019;19: 262.

25. Lustigman S, Prichard RK, Gazzinelli A, Grant WN, Boatin BA, McCarthy JS, et al. A research agenda for helminth diseases of humans: the problem of helminthiases. PLoS Negl Trop Dis. 2012;6: e1582.

26. Health Organization W. The selection and use of essential medicines: report of the WHO Expert Committee on Selection and Use of Essential Medicines, 2021 (including the 22nd …. [cited 28 Aug 2023]. Available: https://apps.who.int/iris/bitstream/handle/10665/351172/9789240041134-eng.pdf?sequence=1

27. Hahnel, Dilks, Heisler, Andersen. Caenorhabditis elegans in anthelmintic research–Old model, new perspectives. Int J Educ Vocat Guid. 2020. Available: https://www.sciencedirect.com/science/article/pii/S2211320720300312

28. Dilks CM, Hahnel SR, Sheng Q, Long L, McGrath PT, Andersen EC. Quantitative benzimidazole resistance and fitness effects of parasitic nematode beta-tubulin alleles. Int J Parasitol Drugs Drug Resist. 2020;14: 28–36.

29. Dilks CM, Koury EJ, Buchanan CM, Andersen EC. Newly identified parasitic nematode

bioRxiv preprint doi: https://doi.org/10.1101/2024.02.01.578300; this version posted February 6, 2024. The copyright holder for this preprint (which was not certified by peer review) is the author/funder, who has granted bioRxiv a license to display the preprint in perpetuity. It is made available under aCC-BY-NC 4.0 International license.

beta-tubulin alleles confer resistance to benzimidazoles. Int J Parasitol Drugs Drug Resist. 2021;17: 168–175.

30. Wit J, Dilks CM, Andersen EC. Complementary Approaches with Free-living and Parasitic Nematodes to Understanding Anthelmintic Resistance. Trends Parasitol. 2021;37: 240–250.

31. Kwok TCY, Ricker N, Fraser R, Chan AW, Burns A, Stanley EF, et al. A small-molecule screen in C. elegans yields a new calcium channel antagonist. Nature. 2006;441: 91–95.

32. Lemieux GA, Liu J, Mayer N, Bainton RJ, Ashrafi K, Werb Z. A whole-organism screen identifies new regulators of fat storage. Nat Chem Biol. 2011;7: 206–213.

33. Leung CK, Wang Y, Malany S, Deonarine A, Nguyen K, Vasile S, et al. An ultra high-throughput, whole-animal screen for small molecule modulators of a specific genetic pathway in Caenorhabditis elegans. PLoS One. 2013;8: e62166.

34. Andersen EC, Shimko TC, Crissman JR, Ghosh R, Bloom JS, Seidel HS, et al. A Powerful New Quantitative Genetics Platform, Combining Caenorhabditis elegans High-Throughput Fitness Assays with a Large Collection of Recombinant Strains. G3 . 2015;5: 911–920.

35. Crombie TA, McKeown R, Moya ND, Evans KS, Widmayer SJ, LaGrassa V, et al. CaeNDR, the Caenorhabditis Natural Diversity Resource. Nucleic Acids Res. 2023. doi:10.1093/nar/gkad887

36. Cook DE, Zdraljevic S, Roberts JP, Andersen EC. CeNDR, the Caenorhabditis elegans natural diversity resource. Nucleic Acids Res. 2017;45: D650–D657.

37. Shaver AO, Wit J, Dilks CM, Crombie TA, Li H, Aroian RV, et al. Variation in anthelmintic responses are driven by genetic differences among diverse C. elegans wild strains. PLoS Pathog. 2023;19: e1011285.

38. Zamanian M, Cook DE, Zdraljevic S, Brady SC, Lee D, Lee J, et al. Discovery of genomic intervals that underlie nematode responses to benzimidazoles. PLoS Negl Trop Dis. 2018;12: e0006368.

39. Pallotto LM, Dilks CM, Park Y-J, Smit RB, Lu BT, Gopalakrishnan C, et al. Interactions of Caenorhabditis elegans β-tubulins with the microtubule inhibitor and anthelmintic drug albendazole. Genetics. 2022;221. doi:10.1093/genetics/iyac093

40. Evans KS, van Wijk MH, McGrath PT, Andersen EC, Sterken MG. From QTL to gene: C. elegans facilitates discoveries of the genetic mechanisms underlying natural variation. Trends Genet. 2021;37: 933–947.

41. Evans KS, Wit J, Stevens L, Hahnel SR, Rodriguez B, Park G, et al. Two novel loci underlie natural differences in Caenorhabditis elegans abamectin responses. PLoS Pathog. 2021;17: e1009297.

42. Gibson SB, Ness-Cohn E, Andersen EC. Benzimidazoles cause lethality by inhibiting the function of Caenorhabditis elegans neuronal beta-tubulin. bioRxiv. 2022. p. 2022.07.21.500991. doi:10.1101/2022.07.21.500991

43. Hahnel SR, Zdraljevic S, Rodriguez BC, Zhao Y, McGrath PT, Andersen EC. Extreme

bioRxiv preprint doi: https://doi.org/10.1101/2024.02.01.578300; this version posted February 6, 2024. The copyright holder for this preprint (which was not certified by peer review) is the author/funder, who has granted bioRxiv a license to display the preprint in perpetuity. It is made available under aCC-BY-NC 4.0 International license.

allelic heterogeneity at a Caenorhabditis elegans beta-tubulin locus explains natural resistance to benzimidazoles. PLoS Pathog. 2018;14: e1007226.

44. Driscoll M, Dean E, Reilly E, Bergholz E, Chalfie M. Genetic and molecular analysis of a Caenorhabditis elegans beta-tubulin that conveys benzimidazole sensitivity. J Cell Biol. 1989;109: 2993–3003.

45. Avramenko RW, Redman EM, Melville L, Bartley Y, Wit J, Queiroz C, et al. Deep amplicon sequencing as a powerful new tool to screen for sequence polymorphisms associated with anthelmintic resistance in parasitic nematode populations. Int J Parasitol. 2019;49: 13–26.

46. Mohammedsalih KM, Krücken J, Khalafalla A, Bashar A, Juma F-R, Abakar A, et al. New codon 198 β-tubulin polymorphisms in highly benzimidazole resistant Haemonchus contortus from goats in three different states in Sudan. Parasit Vectors. 2020;13: 114.

47. Kwa MSG, Kooyman FNJ, Boersema JH, Roos MH. Effect of Selection for Benzimidazole Resistance in Haemonchus contortus on β-Tubulin Isotype 1 and Isotype 2 Genes. Biochem Biophys Res Commun. 1993;191: 413–419.

48. Kwa MSG, Veenstra JG, Roos MH. Molecular characterisation of β-tubulin genes present in benzimidazole-resistant populations of Haemonchus contortus. Mol Biochem Parasitol. 1993;60: 133–143.

49. Kwa MSG, Veenstra JG, Van Dijk M, Roos MH. β-Tubulin Genes from the Parasitic NematodeHaemonchus contortusModulate Drug Resistance inCaenorhabditis elegans. J Mol Biol. 1995;246: 500–510.

50. Silvestre A, Humbert JF. Diversity of benzimidazole-resistance alleles in populations of small ruminant parasites. Int J Parasitol. 2002;32: 921–928.

51. Winterrowd CA, Pomroy WE, Sangster NC, Johnson SS, Geary TG. Benzimidazole-resistant β-tubulin alleles in a population of parasitic nematodes (Cooperia oncophora) of cattle. Vet Parasitol. 2003;117: 161–172.

52. Grant WN, Mascord LJ. Beta-tubulin gene polymorphism and benzimidazole resistance in trichostrongylus colubriformis. Int J Parasitol. 1996;26: 71–77.

53. Martin RJ, Robertson AP, Choudhary S. Ivermectin: An Anthelmintic, an Insecticide, and Much More. Trends Parasitol. 2021;37: 48–64.

54. Holden-Dye L, Walker RJ. Actions of glutamate and ivermectin on the pharyngeal muscle of Ascaridia galli: a comparative study with Caenorhabditis elegans. Int J Parasitol. 2006;36: 395–402.

55. Yates DM, Portillo V, Wolstenholme AJ. The avermectin receptors of Haemonchus contortus and Caenorhabditis elegans. Int J Parasitol. 2003;33: 1183–1193.

56. Brownlee DJ, Holden-Dye L, Walker RJ. Actions of the anthelmintic ivermectin on the pharyngeal muscle of the parasitic nematode, Ascaris suum. Parasitology. 1997;115 (Pt 5): 553–561.

57. Cully DF, Vassilatis DK, Liu KK, Paress PS, Van der Ploeg LH, Schaeffer JM, et al. Cloning of an avermectin-sensitive glutamate-gated chloride channel from Caenorhabditis elegans.

bioRxiv preprint doi: https://doi.org/10.1101/2024.02.01.578300; this version posted February 6, 2024. The copyright holder for this preprint (which was not certified by peer review) is the author/funder, who has granted bioRxiv a license to display the preprint in perpetuity. It is made available under aCC-BY-NC 4.0 International license.

967 Nature. 1994;371: 707–711.

968 58. Dent JA, Davis MW, Avery L. avr-15 encodes a chloride channel subunit that mediates
969 inhibitory glutamatergic neurotransmission and ivermectin sensitivity in Caenorhabditis
970 elegans. EMBO J. 1997;16: 5867–5879.

971 59. Horoszok L, Raymond V, Sattelle DB, Wolstenholme AJ. GLC-3: a novel fipronil and BIDN-
972 sensitive, but picrotoxinin-insensitive, L-glutamate-gated chloride channel subunit from
973 Caenorhabditis elegans. Br J Pharmacol. 2001;132: 1247–1254.

974 60. Dent JA, Smith MM, Vassilatis DK, Avery L. The genetics of ivermectin resistance in
975 Caenorhabditis elegans. Proc Natl Acad Sci U S A. 2000;97: 2674–2679.

976 61. Wolstenholme AJ, Rogers AT. Glutamate-gated chloride channels and the mode of action
977 of the avermectin/milbemycin anthelmintics. Parasitology. 2005;131 Suppl: S85–95.

978 62. Wolstenholme AJ, Neveu C. The avermectin/milbemycin receptors of parasitic nematodes.
979 Pestic Biochem Physiol. 2022;181: 105010.

980 63. Orr HA. Fitness and its role in evolutionary genetics. Nat Rev Genet. 2009;10: 531–539.

981 64. Zimmer C, Emlen DJ. Evolution: making sense of life. Roberts and Company Publishers.
982 Inc Greenwood Village, CO.

983 65. Zhao Y, Long L, Xu W, Campbell RF, Large EE, Greene JS, et al. Changes to social
984 feeding behaviors are not sufficient for fitness gains of the Caenorhabditis elegans N2
985 reference strain. eLife. 2018. doi:10.7554/elife.38675

986 66. Zhang G, Mostad JD, Andersen EC. Natural variation in fecundity is correlated with
987 species-wide levels of divergence in Caenorhabditis elegans. G3 . 2021;11.
988 doi:10.1093/g3journal/jkab168

989 67. Harder A. The Biochemistry of Haemonchus contortus and Other Parasitic Nematodes. Adv
990 Parasitol. 2016;93: 69–94.

991 68. Ghosh R, Andersen EC, Shapiro JA, Gerke JP, Kruglyak L. Natural variation in a chloride
992 channel subunit confers avermectin resistance in C. elegans. Science. 2012;335: 574–578.

993 69. Burga A, Ben-David E, Vergara TL, Boocock J, Kruglyak L. Fast genetic mapping of
994 complex traits in C. elegans using millions of individuals in bulk. doi:10.1101/428870

995 70. O'Halloran DM. Database of glutamate-gated chloride (GluCl) subunits across 125
996 nematode species: patterns of gene accretion and sequence diversification. G3 . 2022;12.
997 doi:10.1093/g3journal/jkab438

998 71. Beech RN, Silvestre A. Mutations Associated with Anthelmintic Drug Resistance. Anti-Infect
999 Agents Med Chem. 2010;9: 105–112.

1000 72. Khan S, Nisar A, Yuan J, Luo X, Dou X, Liu F, et al. A Whole Genome Re-Sequencing
1001 Based GWA Analysis Reveals Candidate Genes Associated with Ivermectin Resistance in
1002 Haemonchus contortus. Genes . 2020;11. doi:10.3390/genes11040367

1003 73. Williamson SM, Storey B, Howell S, Harper KM, Kaplan RM, Wolstenholme AJ. Candidate

bioRxiv preprint doi: https://doi.org/10.1101/2024.02.01.578300; this version posted February 6, 2024. The copyright holder for this preprint (which was not certified by peer review) is the author/funder, who has granted bioRxiv a license to display the preprint in perpetuity. It is made available under aCC-BY-NC 4.0 International license.

anthelmintic resistance-associated gene expression and sequence polymorphisms in a triple-resistant field isolate of Haemonchus contortus. Mol Biochem Parasitol. 2011;180: 99–105.

74. Doyle SR, Laing R, Bartley D, Morrison A, Holroyd N, Maitland K, et al. Genomic landscape of drug response reveals mediators of anthelmintic resistance. Cell Rep. 2022;41: 111522.

75. Wever CM, Farrington D, Dent JA. The Validation of Nematode-Specific Acetylcholine-Gated Chloride Channels as Potential Anthelmintic Drug Targets. PLoS One. 2015;10: e0138804.

76. Feng X-P, Hayashi J, Beech RN, Prichard RK. Study of the nematode putative GABA type-A receptor subunits: evidence for modulation by ivermectin. J Neurochem. 2002;83: 870–878.

77. Kellerová P, Matoušková P, Lamka J, Vokřál I, Szotáková B, Zajíčková M, et al. Ivermectin-induced changes in the expression of cytochromes P450 and efflux transporters in Haemonchus contortus female and male adults. Vet Parasitol. 2019;273: 24–31.

78. Krause RM, Buisson B, Bertrand S, Corringer PJ, Galzi JL, Changeux JP, et al. Ivermectin: a positive allosteric effector of the alpha7 neuronal nicotinic acetylcholine receptor. Mol Pharmacol. 1998;53: 283–294.

79. Doyle SR. Improving helminth genome resources in the post-genomic era. Trends Parasitol. 2022 [cited 4 Jul 2022]. Available: https://pubag.nal.usda.gov/catalog/7806127

80. Doyle SR, Tracey A, Laing R, Holroyd N, Bartley D, Bazant W, et al. Genomic and transcriptomic variation defines the chromosome-scale assembly of Haemonchus contortus, a model gastrointestinal worm. Commun Biol. 2020;3: 656.

81. [No title]. [cited 25 Jan 2024]. Available: https://www.researchgate.net/profile/Stephen-Doyle-9/publication/355271368_The_genome_sequence_of_the_Australian_filarial_nematode_Cercopithifilaria_johnstoni/links/6169f67b951b3574c649e76f/The-genome-sequence-of-the-Australian-filarial-nematode-Cercopithifilaria-johnstoni.pdf

82. Montarry J, Mimee B, Danchin EGJ, Koutsovoulos GD, Ste-Croix DT, Grenier E. Recent Advances in Population Genomics of Plant-Parasitic Nematodes. Phytopathology. 2021;111: 40–48.

83. Howe KL, Bolt BJ, Shafie M, Kersey P, Berriman M. WormBase ParaSite - a comprehensive resource for helminth genomics. Mol Biochem Parasitol. 2017;215: 2–10.

84. Howe KL, Bolt BJ, Cain S, Chan J, Chen WJ, Davis P, et al. WormBase 2016: expanding to enable helminth genomic research. Nucleic Acids Res. 2016;44: D774–80.

85. Hammarlund M, Hobert O, Miller DM 3rd, Sestan N. The CeNGEN Project: The Complete Gene Expression Map of an Entire Nervous System. Neuron. 2018;99: 430–433.

86. Schneider CA, Rasband WS, Eliceiri KW. NIH Image to ImageJ: 25 years of image analysis. Nat Methods. 2012;9: 671–675.

87. Vassilieva LL, Lynch M. The rate of spontaneous mutation for life-history traits in

bioRxiv preprint doi: https://doi.org/10.1101/2024.02.01.578300; this version posted February 6, 2024. The copyright holder for this preprint (which was not certified by peer review) is the author/funder, who has granted bioRxiv a license to display the preprint in perpetuity. It is made available under aCC-BY-NC 4.0 International license.

1043 Caenorhabditis elegans. Genetics. 1999;151: 119–129.

1044 88. Anderson JL, Albergotti L, Ellebracht B, Huey RB, Phillips PC. Does thermoregulatory
1045 behavior maximize reproductive fitness of natural isolates of Caenorhabditis elegans? BMC
1046 Evol Biol. 2011;11: 157.

1047 89. Nyaanga J, Crombie TA, Widmayer SJ, Andersen EC. easyXpress: An R package to
1048 analyze and visualize high-throughput C. elegans microscopy data generated using
1049 CellProfiler. PLoS One. 2021;16: e0252000.

1050 90. Wählby C, Kamentsky L, Liu ZH, Riklin-Raviv T, Conery AL, O'Rourke EJ, et al. An image
1051 analysis toolbox for high-throughput C. elegans assays. Nat Methods. 2012;9: 714–716.

1052 91. Widmayer SJ, Crombie TA, Nyaanga J, Evans KS, Andersen EC. *C. elegans* toxicant
1053 responses vary among genetically diverse individuals. doi:10.1101/2022.07.19.500602

1054 92. Widmayer SJ, Crombie TA, Nyaanga JN, Evans KS, Andersen EC. C. elegans toxicant
1055 responses vary among genetically diverse individuals. Toxicology. 2022; 153292.

1056 93. Nyaanga J, Andersen EC. Linkage mapping reveals loci that underlie differences in C.
1057 elegans growth. G3 . 2022. doi:10.1093/g3journal/jkac207

1058 94. Packer JS, Zhu Q, Huynh C, Sivaramakrishnan P, Preston E, Dueck H, et al. A lineage-
1059 resolved molecular atlas of C. elegans embryogenesis at single-cell resolution. Science.
1060 2019;365. doi:10.1126/science.aax1971

1061 95. Davis P, Zarowiecki M, Arnaboldi V, Becerra A, Cain S, Chan J, et al. WormBase in 2022—
1062 data, processes, and tools for analyzing Caenorhabditis elegans. Genetics. 2022;220:
1063 iyac003.

bioRxiv preprint doi: https://doi.org/10.1101/2024.02.01.578300; this version posted February 6, 2024. The copyright holder for this preprint (which was not certified by peer review) is the author/funder, who has granted bioRxiv a license to display the preprint in perpetuity. It is made available under aCC-BY-NC 4.0 International license.

SUPPORTING INFORMATION

Quantifying the fitness effects of resistance alleles with and without anthelmintic selection pressure using *Caenorhabditis elegans*

Authors: Amanda O. Shaver[1], Isabella R. Miller[1], Etta S. Schaye[1], Nicolas D. Moya[2], J.B. Collins[1], Janneke Wit[1], Alyssa H. Blanco[1], Fiona M. Shao[1], Elliot J. Andersen[1], Sharik A. Khan[1], Gracie Paredes[1], Erik C. Andersen[2]

Affiliations:

[1] Molecular Biosciences, Northwestern University, Evanston, Illinois, United States of America
[2] Dept. of Biology, Johns Hopkins University, Baltimore, Maryland, United States of America

bioRxiv preprint doi: https://doi.org/10.1101/2024.02.01.578300; this version posted February 6, 2024. The copyright holder for this preprint (which was not certified by peer review) is the author/funder, who has granted bioRxiv a license to display the preprint in perpetuity. It is made available under aCC-BY-NC 4.0 International license.

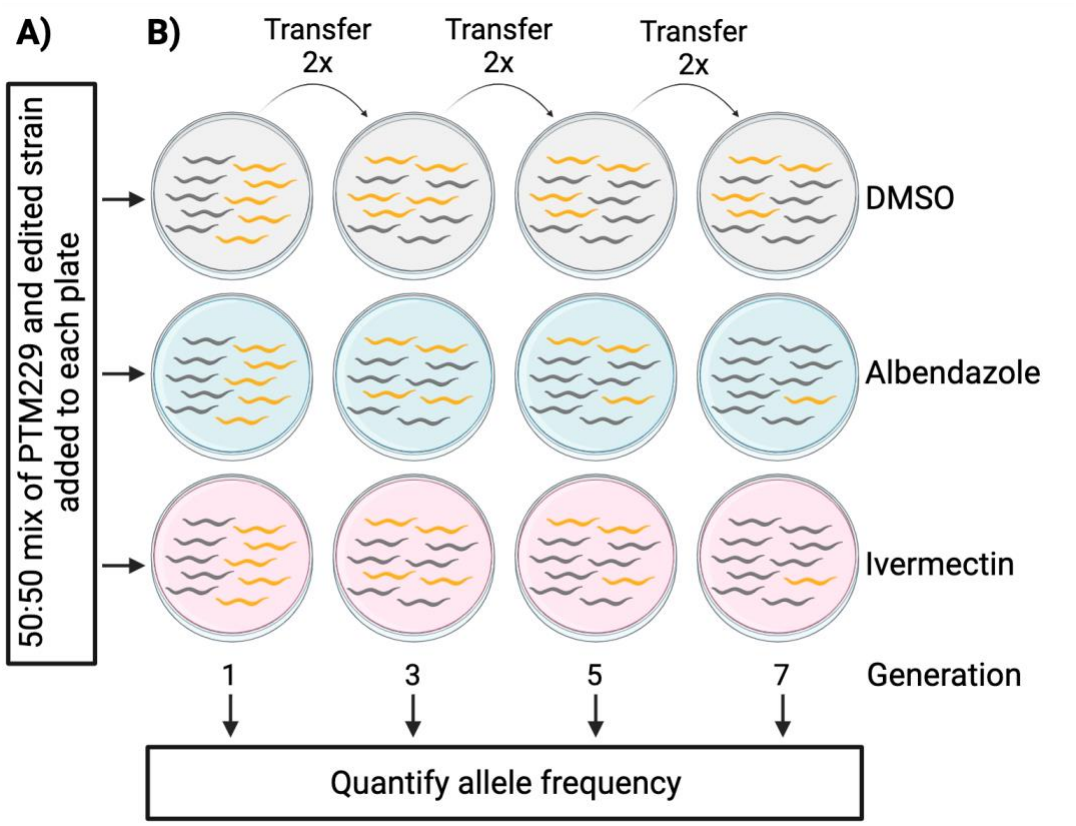

S1 Fig. The competitive fitness assay allows for the assessment of allele frequency in the presence of DMSO, albendazole, or ivermectin.
(A) Equal numbers of the control strain PTM229 were placed on each test plate along with an edited strain. **(B)** Strains were grown on 6 cm NGMA plates for approximately seven days. After seven days, a ~0.5 cm^3 plate chunk of NGMA with animals was transferred to a new 6 cm NGMA plate. Animals were washed off of NGMA plates at each odd generation. After animal collection, DNA extractions, DNA cleanup, and quantification were performed. Allele frequencies were quantified using ddPCR. See *Methods, Competitive fitness assays* for details. Modified from a previous version [65]. Created with Biorender.com.

bioRxiv preprint doi: https://doi.org/10.1101/2024.02.01.578300; this version posted February 6, 2024. The copyright holder for this preprint (which was not certified by peer review) is the author/funder, who has granted bioRxiv a license to display the preprint in perpetuity. It is made available under aCC-BY-NC 4.0 International license.

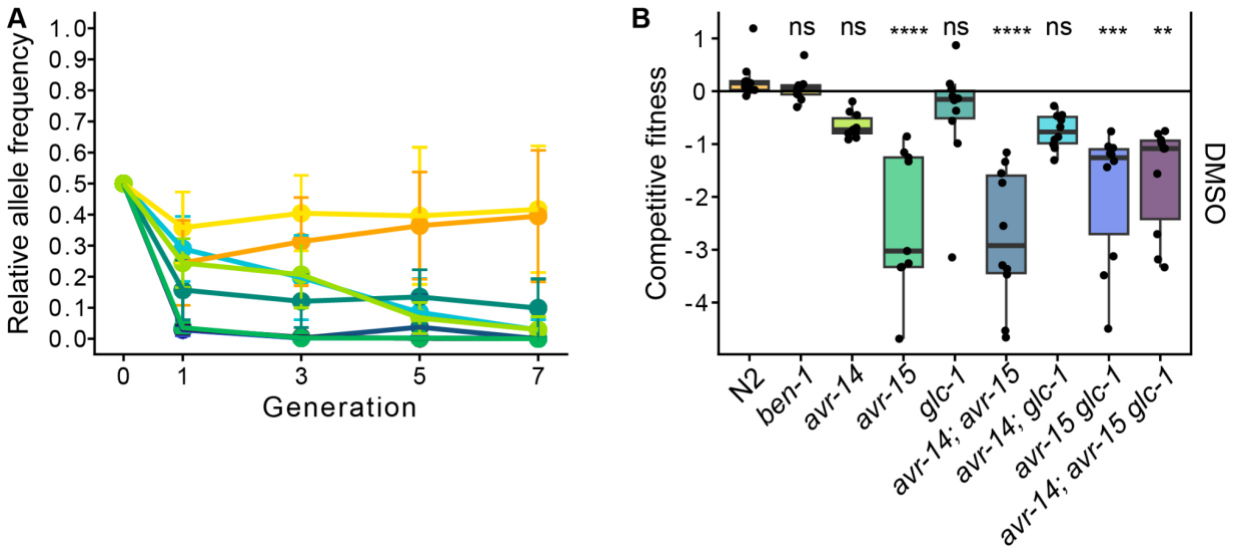

S2 Fig. Competitive fitness assays across seven generations in DMSO.
(A) A barcoded N2 wild-type strain, PTM229, was competed with strains that have deletions in either one, two, or three genes that encode for GluCl channels or in the beta-tubulin gene *ben-1* in DMSO. Generation is shown on the x-axis, and the relative allele frequencies of the nine strains with genome-edited alleles and N2 are shown on the y-axis. **(B)** The $\log_2$-transformed competitive fitness of each allele is plotted in DMSO. The gene tested is shown on the x-axis, and the competitive fitness is shown on the y-axis. Each point represents a biological replicate of that competition experiment. Data are shown as Tukey box plots with the median as a solid horizontal line, and the top and bottom of the box representing the 75th and 25th quartiles, respectively. The top whisker is extended to the maximum point that is within the 1.5 interquartile range from the 75th quartile. The bottom whisker is extended to the minimum point that is within the 1.5 interquartile range from the 25th quartile. Significant differences between the wild-type N2 strain and all the other alleles are shown as asterisks above the data from each strain ($p > 0.05$ = ns, $p < 0.001$ = ***, $p < 0.0001$ = ****, Tukey HSD).

bioRxiv preprint doi: https://doi.org/10.1101/2024.02.01.578300; this version posted February 6, 2024. The copyright holder for this preprint (which was not certified by peer review) is the author/funder, who has granted bioRxiv a license to display the preprint in perpetuity. It is made available under aCC-BY-NC 4.0 International license.

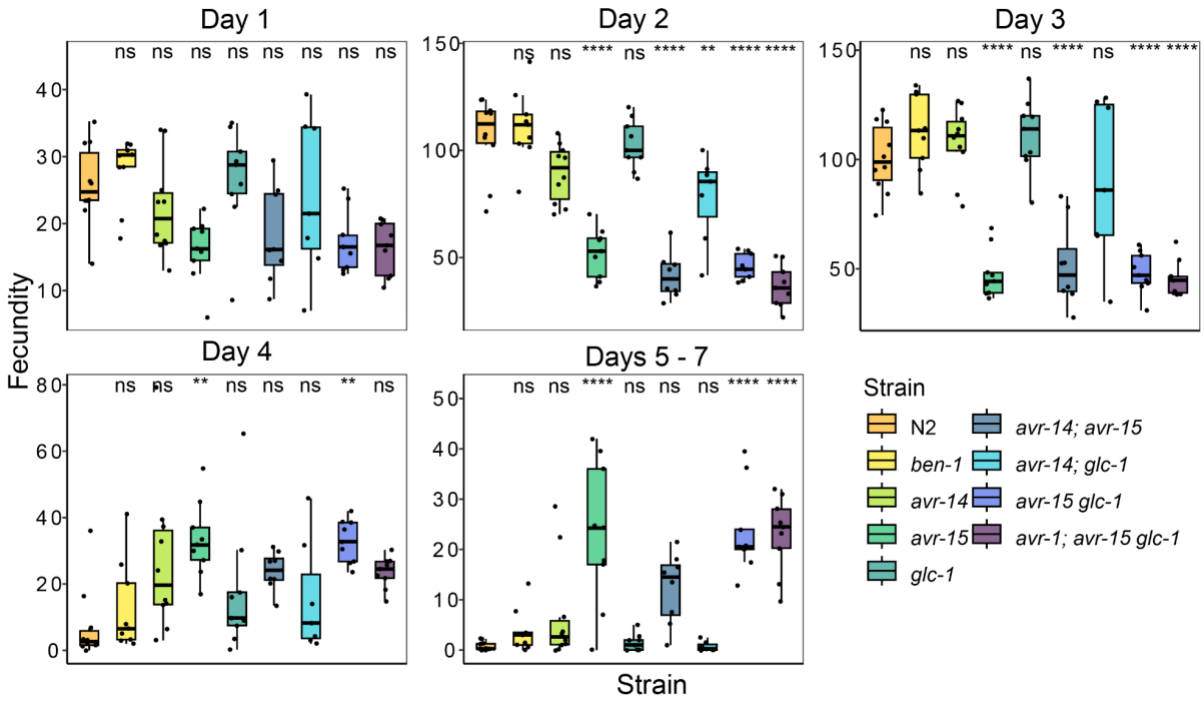

S3 Fig. Variation in daily fecundity of *C. elegans* deletion strains in DMSO. Boxplots for daily fecundity when exposed to DMSO on the y-axis, for each deletion strain on the x-axis. Each point represents the daily fecundity count for one biological replicate. Error bars show the standard deviation of lifetime fecundity among 7 - 10 biological replicates. Data are shown as Tukey box plots with the median as a solid horizontal line, and the top and bottom of the box represent the 75th and 25th quartiles, respectively. Significant differences between the wild-type strain, N2, and all other deletions are shown as asterisks above the data from each strain ($p > 0.05$ = ns, $p < 0.05$ = *, $p < 0.01$ = **, $p < 0.001$ = ***, $p < 0.0001$ = ****, Tukey HSD).

bioRxiv preprint doi: https://doi.org/10.1101/2024.02.01.578300; this version posted February 6, 2024. The copyright holder for this preprint (which was not certified by peer review) is the author/funder, who has granted bioRxiv a license to display the preprint in perpetuity. It is made available under aCC-BY-NC 4.0 International license.

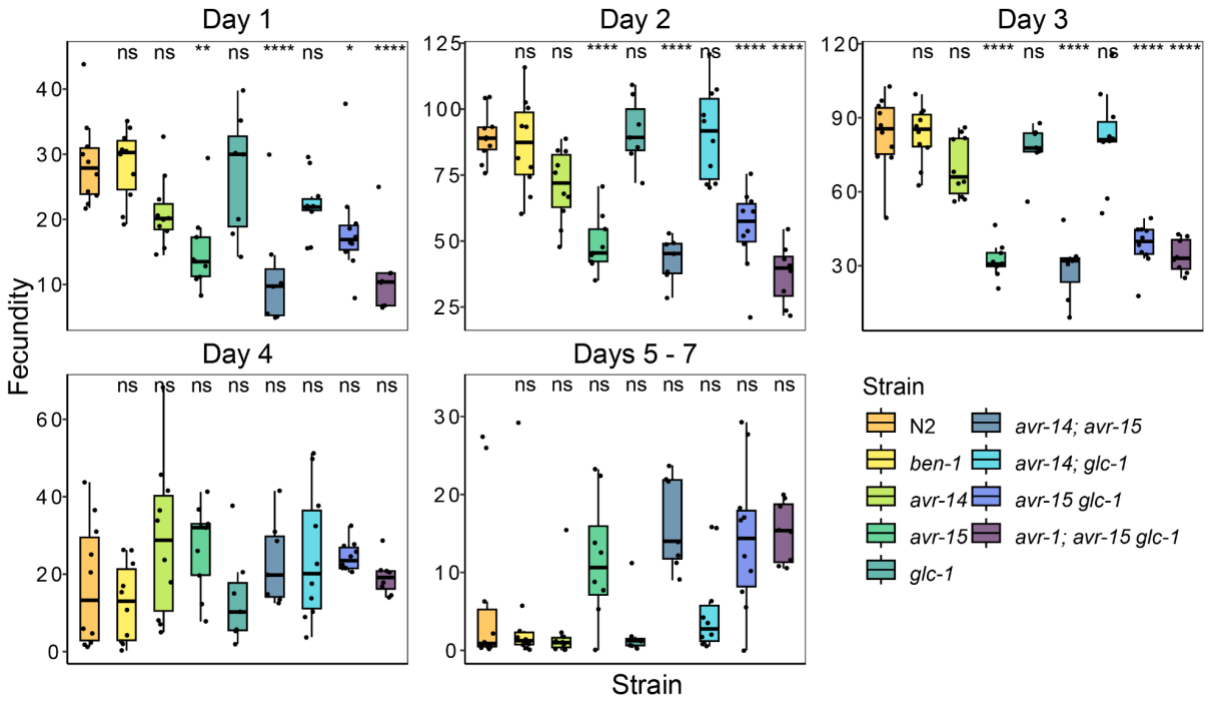

S4 Fig. Variation in daily fecundity of *C. elegans* deletion strains in albendazole. Boxplots for daily fecundity when exposed to albendazole on the y-axis, for each deletion strain on the x-axis. Each point represents the daily fecundity count for one biological replicate. Error bars show the standard deviation of lifetime fecundity among 7 - 10 biological replicates. Data are shown as Tukey box plots with the median as a solid horizontal line, and the top and bottom of the box represent the 75th and 25th quartiles, respectively. Significant differences between the wild-type strain, N2, and all other deletions are shown as asterisks above the data from each strain ($p > 0.05$ = ns, $p < 0.05$ = *, $p < 0.01$ = **, $p < 0.001$ = ***, $p < 0.0001$ = ****, Tukey HSD).

bioRxiv preprint doi: https://doi.org/10.1101/2024.02.01.578300; this version posted February 6, 2024. The copyright holder for this preprint (which was not certified by peer review) is the author/funder, who has granted bioRxiv a license to display the preprint in perpetuity. It is made available under aCC-BY-NC 4.0 International license.

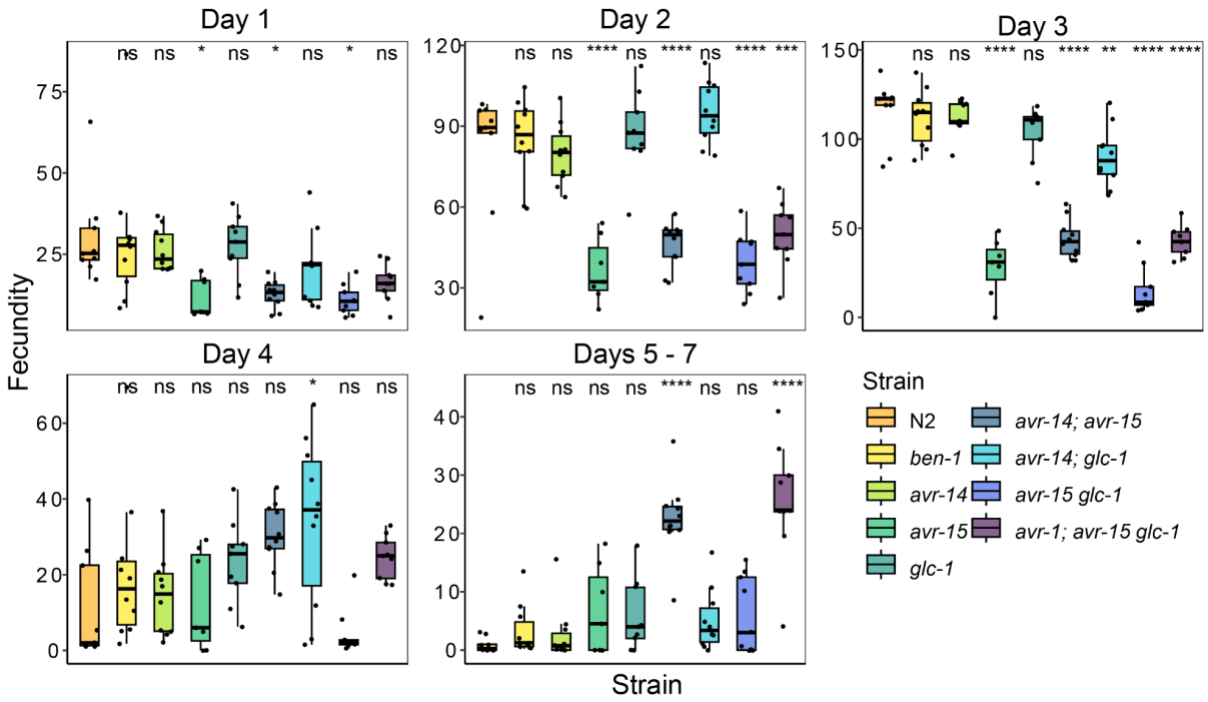

S5 Fig. Variation in daily fecundity of *C. elegans* deletion strains in ivermectin
Boxplots for daily fecundity when exposed to ivermectin on the y-axis, for each deletion strain on the x-axis. Each point represents the daily fecundity count for one biological replicate. Error bars show the standard deviation of lifetime fecundity among 7 - 10 biological replicates. Data are shown as Tukey box plots with the median as a solid horizontal line, and the top and bottom of the box represent the 75th and 25th quartiles, respectively. Significant differences between the wild-type strain, N2, and all other deletions are shown as asterisks above the data from each strain ($p > 0.05$ = ns, $p < 0.05$ = *, $p < 0.01$ = **, $p < 0.001$ = ***, $p < 0.0001$ = ****, Tukey HSD).

bioRxiv preprint doi: https://doi.org/10.1101/2024.02.01.578300; this version posted February 6, 2024. The copyright holder for this preprint (which was not certified by peer review) is the author/funder, who has granted bioRxiv a license to display the preprint in perpetuity. It is made available under aCC-BY-NC 4.0 International license.

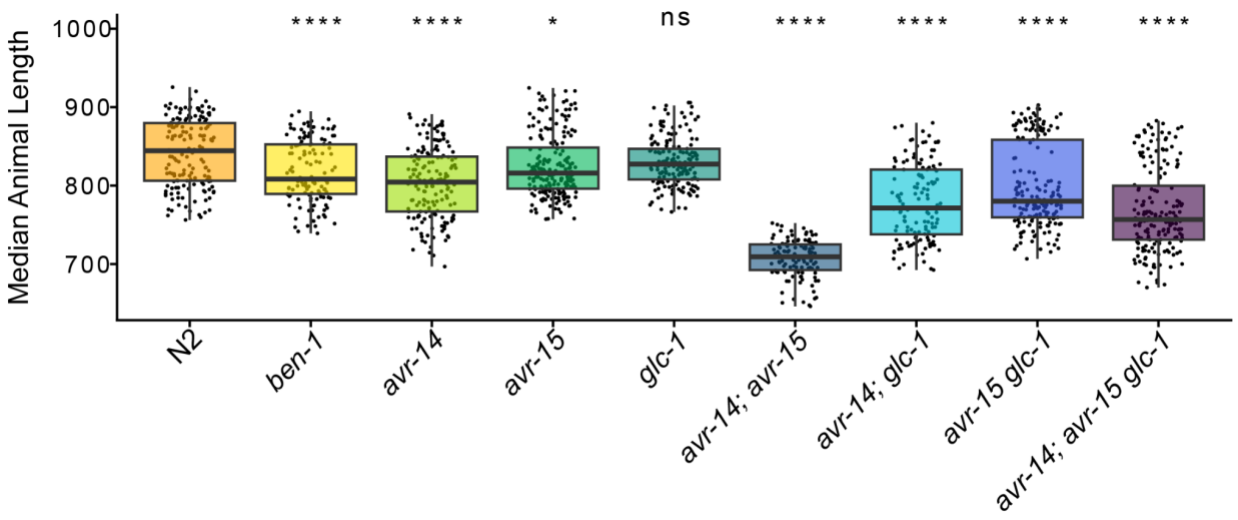

S6 Fig. High-throughput assays for each deletion strain in control conditions. Median animal length values from populations of nematodes grown in DMSO are shown on the y-axis. Each point represents the median animal length from a well containing approximately 5 - 30 animals. Data are shown as Tukey box plots with the median as a solid horizontal line, the top and bottom of the box representing the 75th and 25th quartiles, respectively. The top whisker is extended to the maximum point that is within 1.5 interquartile range from the 75th quartile. The bottom whisker is extended to the minimum point that is within 1.5 interquartile range from the 25th quartile. Significant differences between the wild-type strain and all other strains are shown as asterisks above the data from each strain ($p > 0.05$ = ns, $p < 0.05$ = *, $p < 0.001$ = ***, $p < 0.0001$ = ****, Tukey HSD).

bioRxiv preprint doi: https://doi.org/10.1101/2024.02.01.578300; this version posted February 6, 2024. The copyright holder for this preprint (which was not certified by peer review) is the author/funder, who has granted bioRxiv a license to display the preprint in perpetuity. It is made available under aCC-BY-NC 4.0 International license.

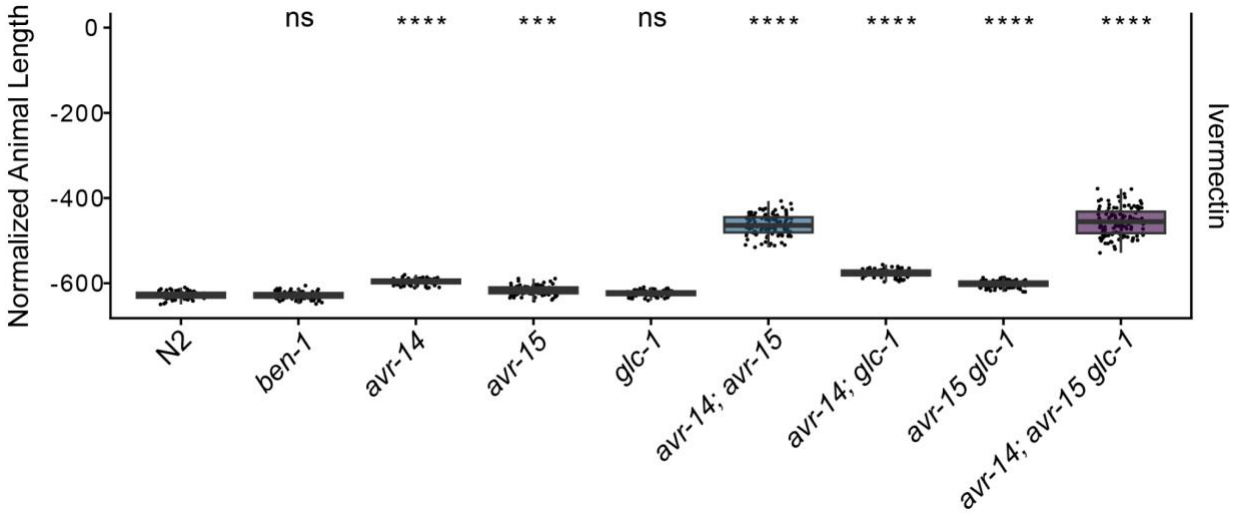

S7 Fig. High-throughput assays for each deletion strain in 500 nM of ivermectin. The regressed median animal length values for populations of nematodes growth in 500 nM ivermectin are shown on the y-axis. Each point represents the regressed median animal length value of a well containing approximately 5-30 animals. Data are shown as Tukey box plots with the median as a solid horizontal line, and the top and bottom of the box representing the 75th and 25th quartiles, respectively. The top whisker is extended to the maximum point that is within the 1.5 interquartile range from the 75th quartile. The bottom whisker is extended to the minimum point that is within the 1.5 interquartile range from the 25th quartile. Significant differences between the wild-type strain and all other deletions are shown as asterisks above the data from each strain ($p > 0.05$ = ns, $p < 0.001$ = ***, $p < 0.0001$ = ****, Tukey HSD).

bioRxiv preprint doi: https://doi.org/10.1101/2024.02.01.578300; this version posted February 6, 2024. The copyright holder for this preprint (which was not certified by peer review) is the author/funder, who has granted bioRxiv a license to display the preprint in perpetuity. It is made available under aCC-BY-NC 4.0 International license.

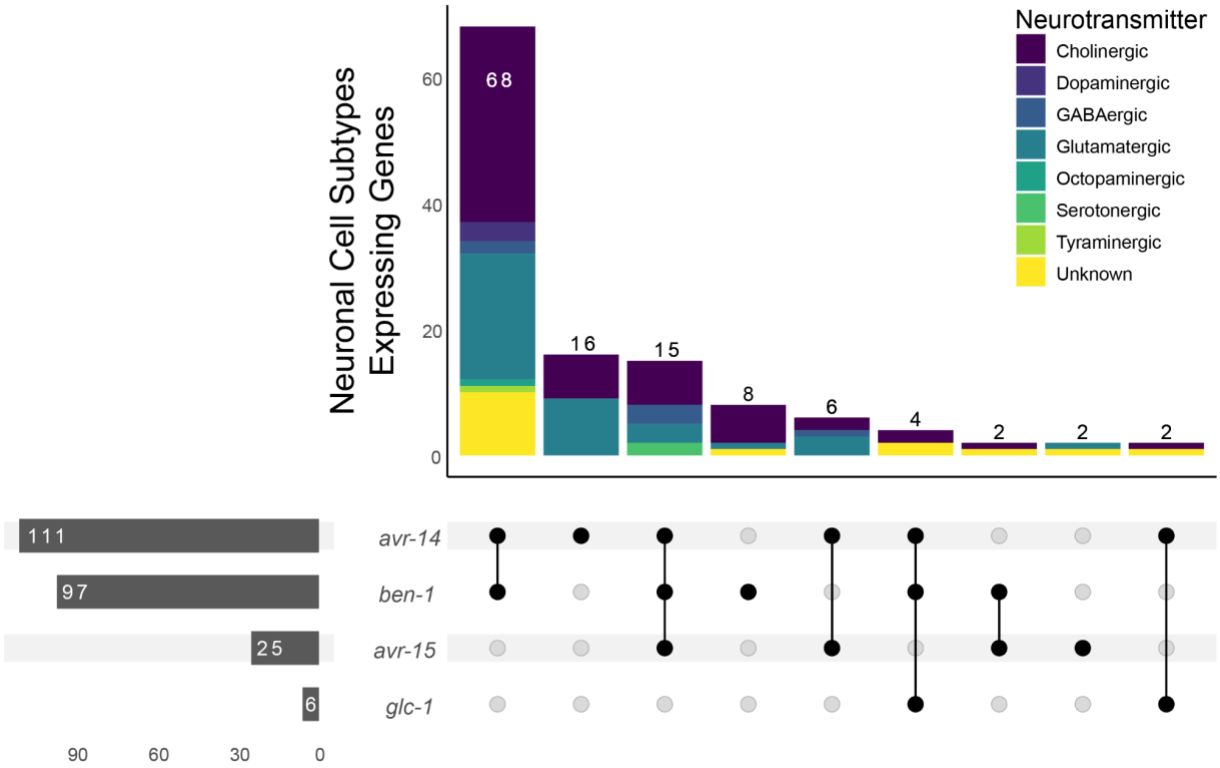

S8 Fig. Upset plot of the neuronal expression patterns for *ben-1*, *avr-14*, *avr-15*, and *glc-1*. Upset plot of single-cell RNA-sequencing data obtained from CeNGEN. Horizontal bar plots sum the total number of neurons where the gene is expressed. Vertical bar plots sum overlap where genes are expressed in the neuronal cell subtypes. Black dots directly under vertical bar plots signify the gene(s) that overlap in the neuronal cell subtypes indicated in the vertical bar plot.

REFERENCES

1. Zhao Y, Long L, Xu W, Campbell RF, Large EE, Greene JS, et al. Changes to social feeding behaviors are not sufficient for fitness gains of the Caenorhabditis elegans N2 reference strain. eLife. 2018. doi:10.7554/elife.38675